THE PERKIN-ELMER CORPORATION

REPORT NO. 9204

ACOUSTIC SELF-TRAPPING OF LASER BEAMS

Final Report

PERKIN-ELMER

THE PERKIN-ELMER CORPORATION

REPORT NO. 9204

ACOUSTIC SELF-TRAPPING OF LASER BEAMS

Final Report

Submitted by

Edwin L. Kerr, Project Scientist
(Phone 203-762-4650)

to the

OFFICE OF NAVAL RESEARCH

ARPA Order Number 306 Project Code Number_____
Contract Number N00014-67-C-0468 Amount $24,079
Contract Duration 1 May 1967 through 29 February 1968

This Research is part of Project DEFENDER under the joint sponsorship of the Advanced Research Projects Agency, the Office of Naval Research, and the Department of Defense.

TABLE OF CONTENTS

TABLE OF CONTENTS (Cont'd.)

LIST OF ILLUSTRATIONS

LIST OF ILLUSTRATIONS (Cont'd.)

ABSTRACT

Internal filamentary glass damage caused by high power Q-switched pulse lasers and filamentary trapping in liquids is analyzed theoretically in this report. Several models are proposed and discussed for electrostrictively driven acoustic trapping. An analysis of Kerr effect trapping is also given for purposes of comparison.

In the acoustic theory, electrostriction is the sound wave driving force. The sound wave compressions cause focusing of the light wave fields. The focused light fields in turn cause stronger electrostriction forces. When the beam power is large enough and the laser pulse duration is approximately equal to the time required for sound to cross the unfocused beam radius, the trapping process runs until the beam is focused to a small radius limited by diffraction.

The theoretical trapping thresholds are calculated from the laser wavelength and the density, refractive index, Young's modulus, and Poisson's ratio of a solid material, or the density, refractive index, and speed of sound of a liquid medium. These thresholds agree with experimental glass damage thresholds to within experimental error, and they vary the same way with initial beam size. Computer movies showing the formation of strongly focused regions are presented. An explanation is given for most of the salient features observed in the damage phenomenon. Mathematical analyses of various features of the models are presented with computed graphs.

SECTION I

PREFACE

The goal of the research reported here is to continue the development of a theory of acoustic beam trapping. The theory is a possible explanation of the mechanism for internal, filamentary glass damage by lasers. It may also be an explanation for some of the beam-trapping phenomena observed in liquids when they are traversed by a high intensity laser pulse.

We began developing the theory in 1965. Sections II and III present theoretical results obtained by August 1966.

Section IV covers an analytical solution to the beam-trapping equations for the case in which Kerr effect trapping is the dominant trapping mechanism and where electrostrictively driven sound waves are weak or absent.

Section V presents some of our computer results, depicting the acoustic beam-trapping phenomenon. An explanation of the salient features of the glass damage phenomenon is given.

Section VI presents derivations of formulas used in the computer programs. It is the summary of work performed in the second half of the contract.

BLANK PAGE

SECTION II

INTRODUCTION

2.1 A NEW POWER LIMIT

As higher and higher power lasers are developed, basic limitations in the power-transmitting capability of materials and propagation media are being discovered. Examples of limitations are electric breakdown and beam instability. During our study of gain saturation and other anomalies in stimulated Raman effect and in our experimental work in laser damage to glass, we have identified a new kind of beam instability, acoustic beam trapping.

Acoustic beam trapping is caused by the focusing action of electrostrictively driven acoustic waves. These waves alter the index of refraction of the medium by the density changes they cause. All optical materials experience these electrostriction forces and photoelastic effects.

Acoustic beam trapping sets upper limits to beam power that can be transmitted in important materials such as glass and air. Furthermore, the scaling laws for acoustic trapping (power threshold versus beam size and pulse half-time) differ from the scaling laws for other types of beam instability, such as Kerr effect or anomalous dispersion trapping. In fact, for many transparent materials, there is a beam size and pulse half-time for which the acoustic trapping threshold is lower than the thresholds for other known instabilities.

2.2 THRESHOLD PREDICTABLE

At the present time, we can predict the acoustic trapping power threshold in glassy materials from a knowledge of material properties, wavelength, pulse half-time, and beam size. There is a minimum power level for each material which can be calculated from tabulated material properties and the laser wavelength.

2.3 RECONCILABLE WITH STEADY STATE TRAPPING THEORY

We have also shown that for any given beam size and type of material, there is a maximum average rate of increase of power that can be transmitted without causing acoustic beam trapping. So long as power is added to a beam at a slower rate than this, it is possible in principle to reach the steady state trapping threshold predicted by Chiao, Garmire, and Townes (Ref. 1).

2.4 SCALING LAWS

Figure 1 illustrates the scaling laws for three different effects that limit the ability of an optical material to transmit a laser beam. In the graph, total beam power is plotted versus beam radius on log-log scales. The three effects are electric field breakdown, Kerr effect trapping, and acoustic trapping.

For electric field breakdown, as in laser-induced "air sparks,"

$$\text{Power Threshold for Breakdown} = \left(\text{Constant for Material}\right)\left(\text{Beam Radius}\right)^2$$

On the log-log plot, this power threshold is a line with a slope of 2. Thus, electric field breakdown limits the material to transmission of power levels and beam sizes in the right-hand portion of the graph.

For Kerr effect trapping, as shown by Chiao, Garmire, and Townes (Ref. 1)

$$\text{Power Threshold for Kerr Effect Trapping} = (\text{Wavelength})\left(\text{Constant for Material}\right)$$

Since the threshold is independent of beam size, it appears as a horizontal line on the graph. For transmission without Kerr effect trapping, the beam power level must be below the Kerr effect threshold.

Together, Kerr effect trapping and electric field breakdown limit beam transmission to beam sizes and power levels in the lower right portion of the graph. Both of the effects are virtually independent of the pulse half-time.

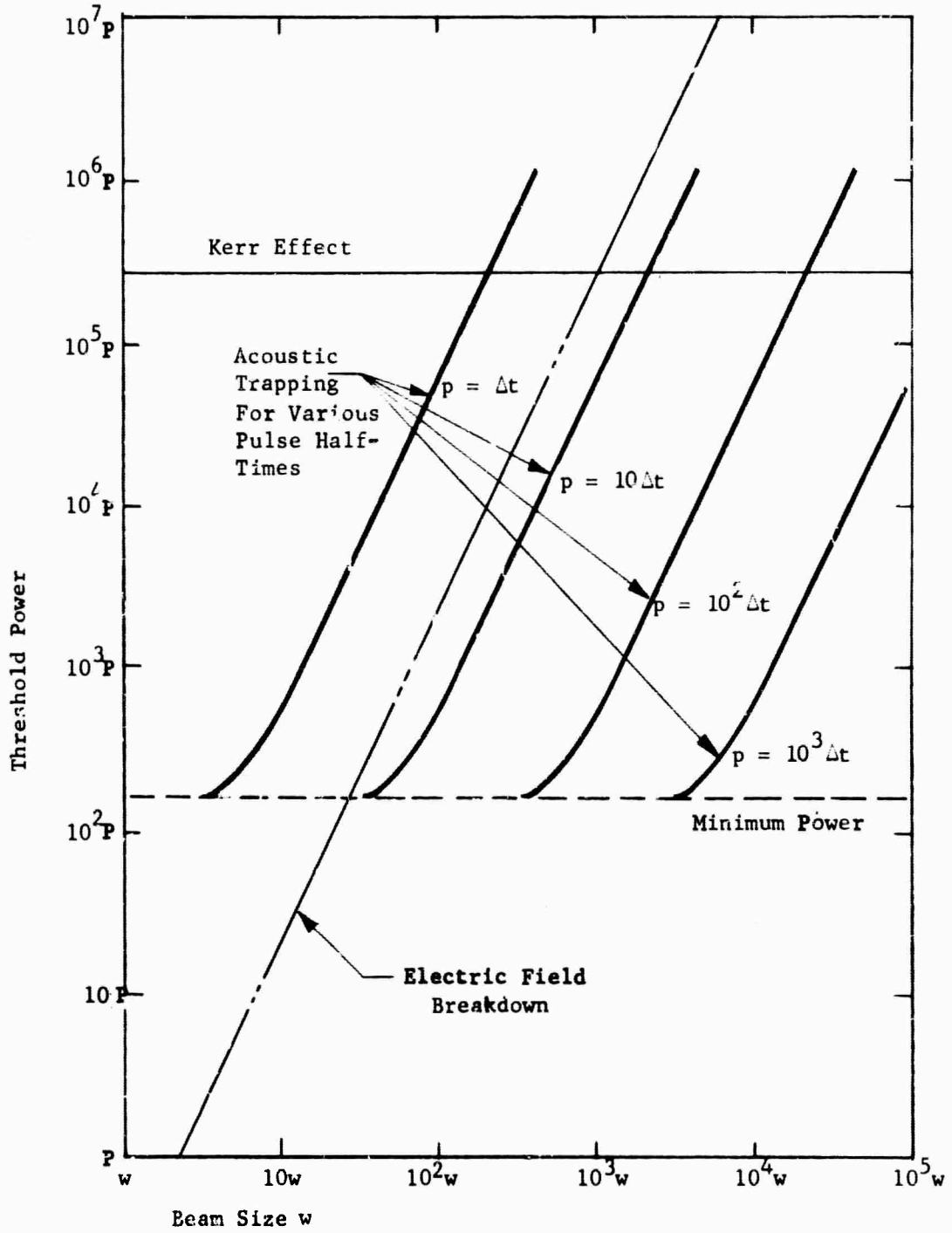

Figure 1. Scaling Laws for Kerr Effect Trapping, Breakdown, and Acoustic Trapping.

The acoustic trapping threshold can be calculated as in Section III as long as the laser pulse half-time, p, is less than the time required for sound to cross the beam radius. The scaling law for acoustic trapping is

$$\text{Power Threshold for Acoustic Trapping} = (\text{Wavelength})^2 \left(\text{Constant for Material} \right) \frac{(\text{Beam Radius})^2}{(\text{Pulse Half-time})^2}$$

for the limiting case of a very short pulse or a very large beam. If the pulse half-time is held constant, the threshold power can be plotted versus beam size as shown in the graph. The acoustic trapping power threshold curve flattens out at the bottom, at the minimum power level. This minimum power level, P_{min}, is characteristic only of the material and the wavelength.

For the domain in which the pulse half-time is longer than the time T required for sound to cross the beam, the acoustic trapping threshold remains at P_{min}. This power level can be exceeded only if the power does not increase more rapidly than P_{min}/T in any time T.

If the pulse half-time is increased by a numerical factor, and the beam radius is increased by the same factor, the power threshold remains constant. Thus, in the log-log graph, the curve is shifted to the right by the log of the numerical factor by which the beam radius is increased. Thus the graph shows three extra curves shifted by factors of 10, 100, and 1000.

In some materials the Kerr effect trapping threshold is lower than the minimum power level for acoustic trapping. In these materials Kerr effect trapping will occur before acoustic trapping. However, most common optical materials have a critical power level lower than the Kerr effect trapping threshold. For these materials there will always be a domain of beam size and pulse half-time in which acoustic beam trapping sets the maximum transmittable power for the material.

2.5 TYPICAL RESULTS FOR GLASS

Acoustic trapping is an important cause of laser damage to optical glass, as shown in experiments performed by Steinberg, Atwood, Lee, and Ward (Ref. 2). The theoretical trapping threshold is compared with the experimental

damage threshold in Figure 2. Generally, the trapping threshold is below the experimental damage threshold points, as expected. In particular, note the experimental damage threshold curve for dense flint. The left, lower portion has a slope of 2. In that region, the cause of damage is probably electric breakdown. The right, upper portion fits the curve for acoustic trapping to within the experimental repeatability, and it scales the same way. For fused silica and BK-7 the agreement between the acoustic trapping threshold and the measured damage threshold is even better.

The experimental results are not attributable to Kerr effect trapping because of the dependence on beam size. Also, in glass, Kerr effect is so weak that the power threshold for Kerr effect trapping is 4 megawatts, which is above the top of the graph.

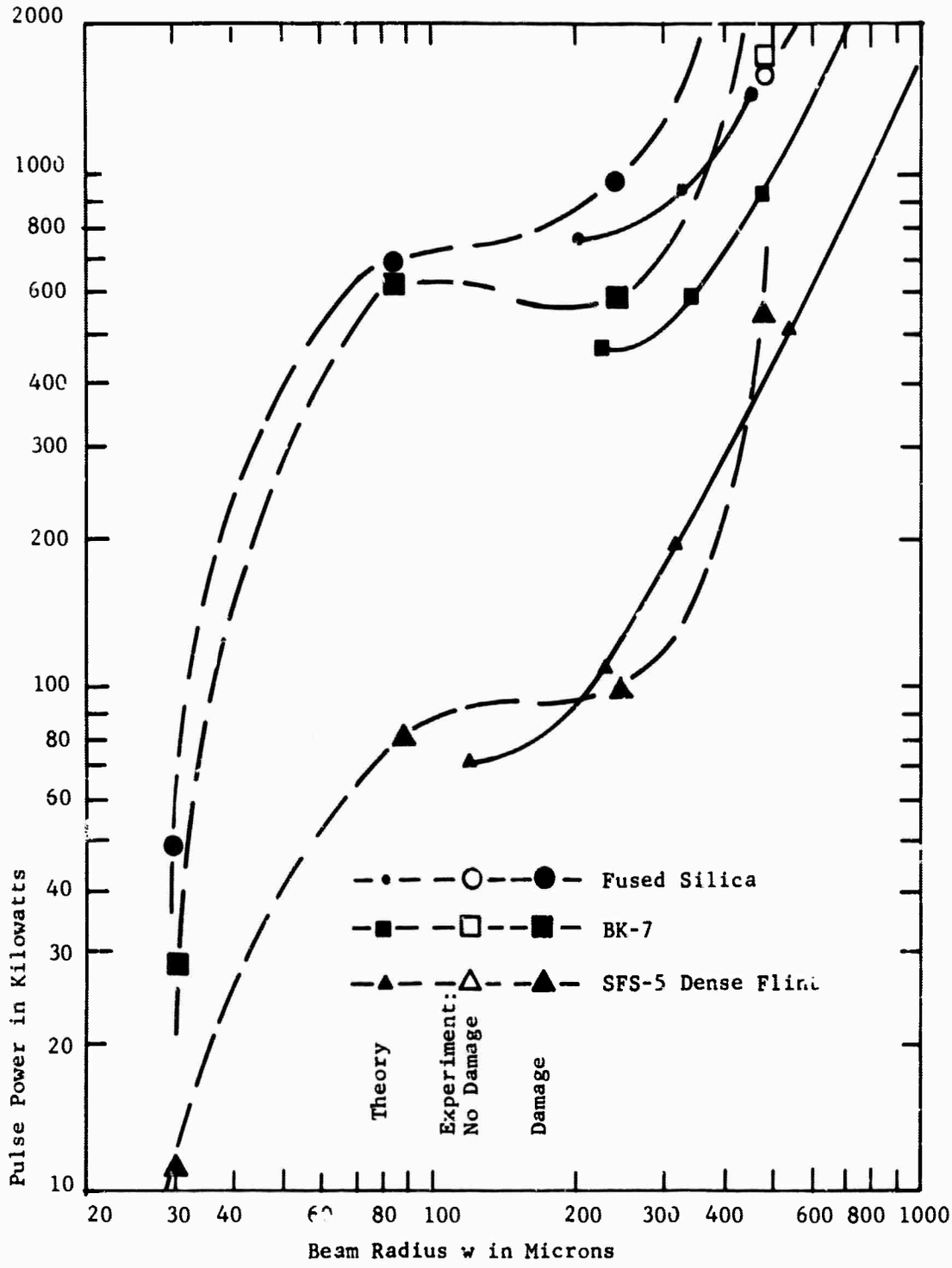

Figure 2. Laser Damage Thresholds for Three Optical Glasses

SECTION III

DERIVATION OF THE ACOUSTIC BEAM TRAPPING THRESHOLD

3.1 THE DRIVING FORCE

Electrostriction is the force exerted by an electric field on a material medium, when the force is proportional to the square of the field. The net body force is then proportional to the power intensity gradient, in a lossless medium. The relevant permittivity ratio at optical frequencies is the square of the refractive index. Thus, the net body force $\bar{f}$ per unit volume due to the light beam is (Ref. 3)

$$\bar{f} = (1/6n_o c)\ (n_o^2 + 2)\ (n_o^2 - 1)\ \bar{\nabla} I.$$

Thus a cylindrical beam will drive a radially propagating sound wave.

3.2 THE PHOTOELASTIC EFFECT

The refractive index change Δn due to small acoustic compressions is defined as

$$\Delta n = n - n_o = (\rho - \rho_o)\ \partial n/\partial \rho$$

Assuming constant polarizability per molecule, $\partial n/\partial \rho$ may be calculated by differentiating the Clausius-Mosotti relation. Then we obtain

$$\Delta n = (1/6\ n_o)(n_o^2 + 2)(n_o^2 - 1)\ \sigma$$

where σ is the normalized compression.

$$\sigma = (\rho - \rho_o)/\rho_o$$

Other effects, such as the Kerr effect, may add to Δn. They will not have the same distribution as acoustic compression, in general, nor will they vary the same way with beam size. However, they can be added to Δn later. Let us ignore them for the present.

3.3 THE LASER BEAM

For the purpose of this discussion, the laser pulse is represented by two impulses of equal energy. Each impulse has a Gaussian radial intensity distribution. The radius is measured to the point where the intensity drops to 1/e of the peak intensity. The beam is circularly symmetrical and gently focused. At the focus the intensity distribution is

$$I(r,t) = (W/\pi w^2) \exp(-r^2/w^2)\left[\delta(t) + \delta(t-\Delta t)\right]/2$$

where W is the energy of two impulses. The two impulses are separated by a time, Δt, equal to 2/3 the half-height duration or half-time, p, of the laser pulse. Thus if the physical laser pulse has a Gaussian time distribution, the two impulses will occur at the centroids of the two halves of the physical pulse.

The temporal intensity distribution is shown in Figure 3, and the spatial intensity distribution is sketched in Figure 4. The resulting force distribution is given in Figure 5.

3.4 THE ACOUSTIC WAVE

The electrostrictive force drives a radially propagating acoustic wave. Usually when acoustic beam trapping occurs the boundaries of the material are so far from the beam center that the trapping event occurs sooner than sound can be reflected from the boundaries. Hence, the acoustic wave equation applies with the following conditions:

1) Circular symmetry
2) Infinite homogeneous isotropic medium
3) Solution at the beam center is well behaved
4) Solution at infinite radius is zero
5) Solution is not a function of z (paraxial beam case)

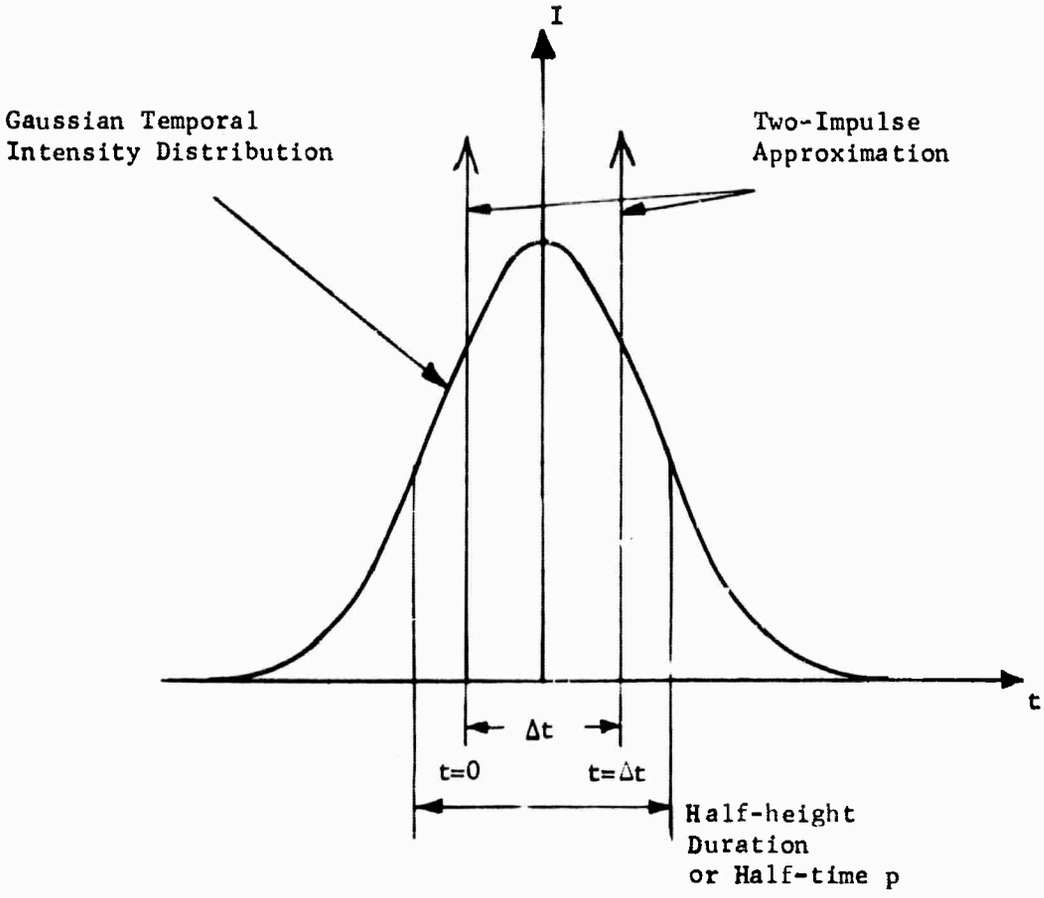

Figure 3. Laser Pulse Temporal Intensity Distribution, and the Two-Impulse Approximation.

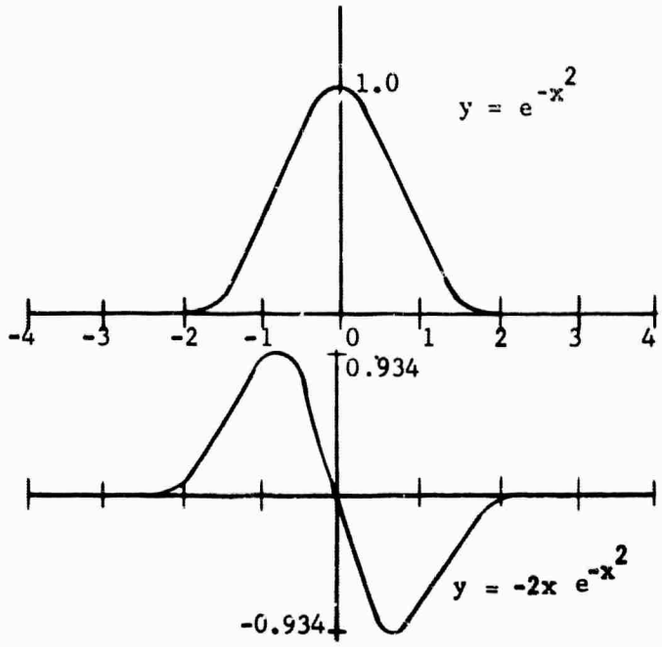

Figure 4.

Gaussian Spatial Intensity Distribution

Figure 5.

Initial Force Distribution

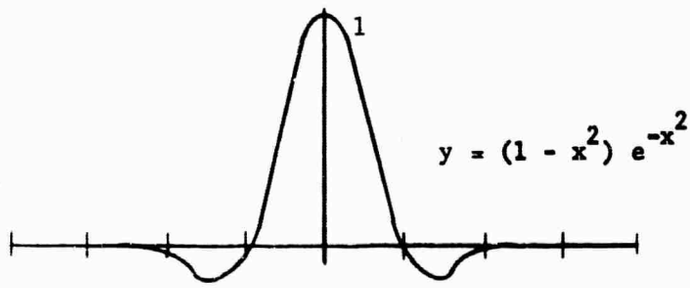

Figure 6.

Initial Rate of Change of Compression Distribution

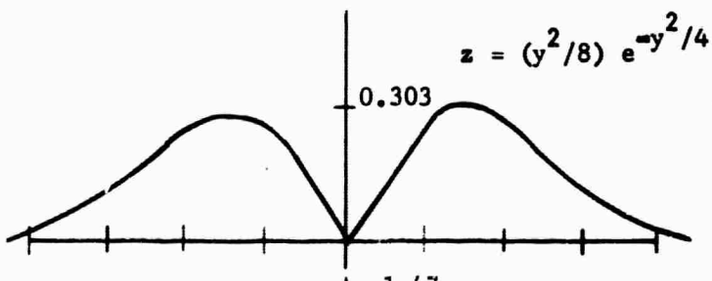

Figure 7.

Hankel Transform of Initial Rate of Change of Compression

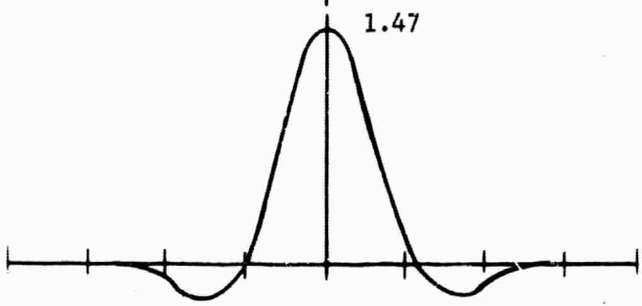

Figure 8.

Acoustic Compression at $\tau = 0.596$. Proportional to Refractive Index Change

The acoustic wave equation can be solved for the case of an impulse driving force. Since the equation is linear, it is convenient to use dimensionless variables and a normalized impulse.

Let the dimensionless radial coordinate be x, the radius measured in units of the initial focused beam radius w;

$$x = r/w$$

There is a characteristic acoustic response time, T, equal to the time required for sound to traverse the beam radius;

$$T = w/v$$

where v is the speed of sound for a two-dimensional compression wave.

$$v = (Y/2\rho_o)^{1/2} (1 - \epsilon)^{-1/4} \qquad (1)$$

Here Y is Young's modulus and ϵ is Poisson's ratio for solid media.

Let the dimensionless time variable be τ, time measured in units of T.

$$\tau = t/T = (v/w)\ t$$

This choice of units makes the velocity of sound equal unity in the wave equation. Also, the acoustic velocity $\dot{\bar{u}}$ is normalized by the velocity of sound, and the acoustic displacement $\bar{u}$ is normalized by w. The acoustic compression σ is the negative divergence of the displacement:

$$\sigma = -\bar{\nabla} \cdot \bar{U}$$

where $\bar{U} = \bar{u}/w$. Differentiating with respect to τ, we have

$$\partial\sigma/\partial\tau = -\bar{\nabla} \cdot \partial\bar{U}/\partial\tau$$

where $\partial U/\partial\tau = \dot{\bar{u}}/v$

The initial rate of change of compression distribution appears in Figure 6.

When the electrostrictive force acts impulsively on a medium initially at rest, there is no immediate displacement or compression. The initial velocity and initial rate of change of compression may be deduced from conservation of momentum,

$$\int_{-\infty}^{0+} \bar{f}\, dt = \rho_o \dot{u}(x, 0+)$$

The compression σ is a function of radius and time only. To sum up, the problem is to solve the acoustic wave equation:

$$\nabla^2 \sigma = \partial^2\sigma/\partial\tau^2$$

subject to

1) $\sigma = \sigma(x, \tau)$

2) $\sigma(x,0) = 0$

3) $\partial\sigma(x,0)/\partial\tau = A(1 - x^2) \exp(-x^2)$

where

$$A = (W/3\pi n_o c v \rho_o w^3)(n_o^2 + 2)(n_o^2 - 1)$$

4) $\sigma(0, \tau) \neq \infty$

5) $\sigma(\infty, \tau) = 0$

The equation and all of the conditions except (3) are satisfied by $\sigma(x, \tau) = (B/A) J_o(yx) \sin(y\tau)$ where B and y are arbitrary. A linear superposition of solutions will satisfy condition (3) as well. The correct combination of solutions g(y) is given by the Hankel transform (not the Fourier transform because of circular symmetry). The weight function is x

and the eigenfunctions are $J_o(yx)$ corresponding to 1 and sin (xy) or cos (yx) for a Fourier transform. Thus,

$$g(y) = \int_o^\infty \xi \left[A(1 - \xi^2) \exp(-\xi^2)\right] J_o(\xi y)\, d\xi$$

$$= A(y^2/8) \exp(-y^2/4)$$

This distribution is plotted in Figure 7. Now superposition is applied to obtain the solution.

$$\sigma(x,\tau) = A \int_o^\infty (y^2/8) \exp(-y^2/4)\, J(yx) \sin(y\tau)\, dy$$

This difficult integral has been evaluated numerically as described below. For the important on-axis case, where x = 0, the integration may be performed analytically, since $J_o(0) = 1$.

$$\sigma(0,\tau) = A \int_o^\infty (y^2/8) \exp(-y^2/4) \sin(y\tau)\, dy$$

$$= A\,\tau/2 + (A/2)(1 - 2\tau^2) \exp(-\tau^2) \int_o^\tau \exp(\xi^2)\, d\xi$$

$$= A(\tau - 4\tau^3/3 + \cdots)$$

This function is plotted in Figure 9.

3.5 THE NUMERICAL INTEGRATION

The integral for $\sigma(x, \tau)$ was computed in our Scientific Computer Facility. We programmed the Scientific Data Systems 9300 Computer with 65 Fortran IV statements. Simpson's method was used. The Bessel function was generated by a polynomial approximation accurate to 5×10^{-8} absolute error from the Handbook of Mathematical Functions (Ref. 4., pp 369f). One hundred and one values of y were used each time the integral was evalutated. The integral was computed at 101 values of x for each of 124 values of τ. Time was saved by storing parts of the kernel that do not change, and by buffering the printer. Running time was about 40 minutes, or about 1 millisecond for each evaluation of the Bessel function.

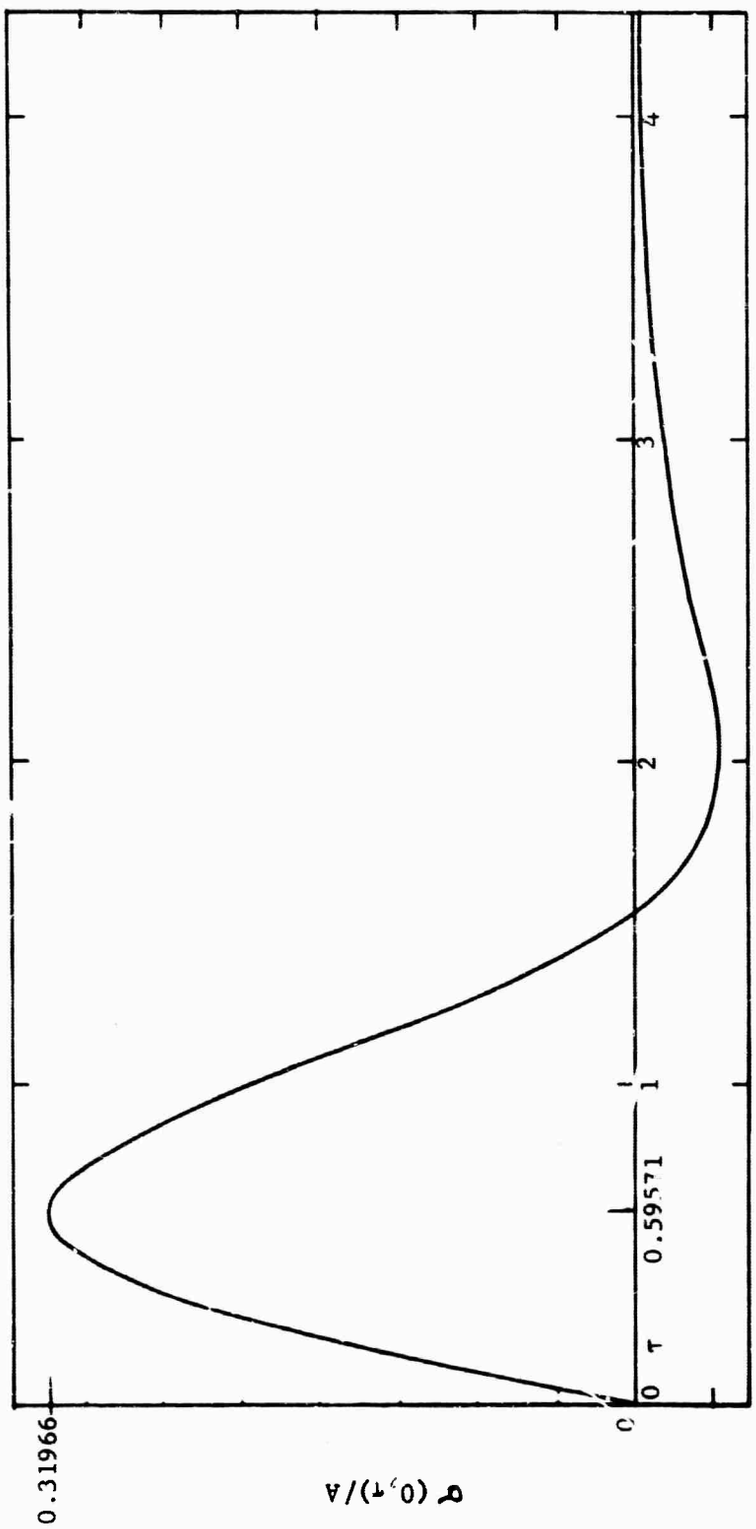

Figure 9. Beam Center Compression as a Function of Time

The computed points were saved on magnetic tape. We displayed the points with the on-line oscilloscope associated with our SDS 930 Computer. The Fortran II display program allowed us to show stationary frames continuously, or to show frames sequentially at any comfortable viewing rate. The display was useful in studying the wave motion and in checking the computation.

Refer to Figures 10 and 11 for plots of wave amplitude σ/A versus x at various values of τ. The compression at maximum on-axis amplitude is plotted in Figure 8, for comparison with the other functions in the solution.

3.6 THE TRAPPING CONDITION

An unexpected result of the computed solution of the acoustic wave is the fact that the compression is greatest on axis, for $0 < \tau < 0.85$. Thus, it is, from the start, a focusing distribution. There is no latency period of zero or negative focusing before some positive focusing begins. The on-axis solution shown in Figure 9 shows that the convergence (reciprocal focal length) varies linearly with τ, for $\tau \ll 1$.

The two-impulse model is valid for $\tau < 0.85$. The first impulse starts an acoustic wave, and the acoustic wave builds up a distributed lens of increasing convergence. Diffraction of the second impulse will be defeated if, at the time the second impulse occurs,

$$\Delta n/n > (1/2)(\lambda/2\pi n_o w)^2.$$

This on-axis Δn will be the sum of Δn caused by the acoustic wave and Kerr effect. The acoustic Δn is a function of beam energy, pulse duration, and initial focused spot size. Kerr effect depends on power. Thus the two effects do not vary the same way with beam size.

3.7 THE TRAPPING THRESHOLD

For optical glass and other materials in which Kerr effect is weak, we may calculate the approximate energy threshold for trapping by equating the

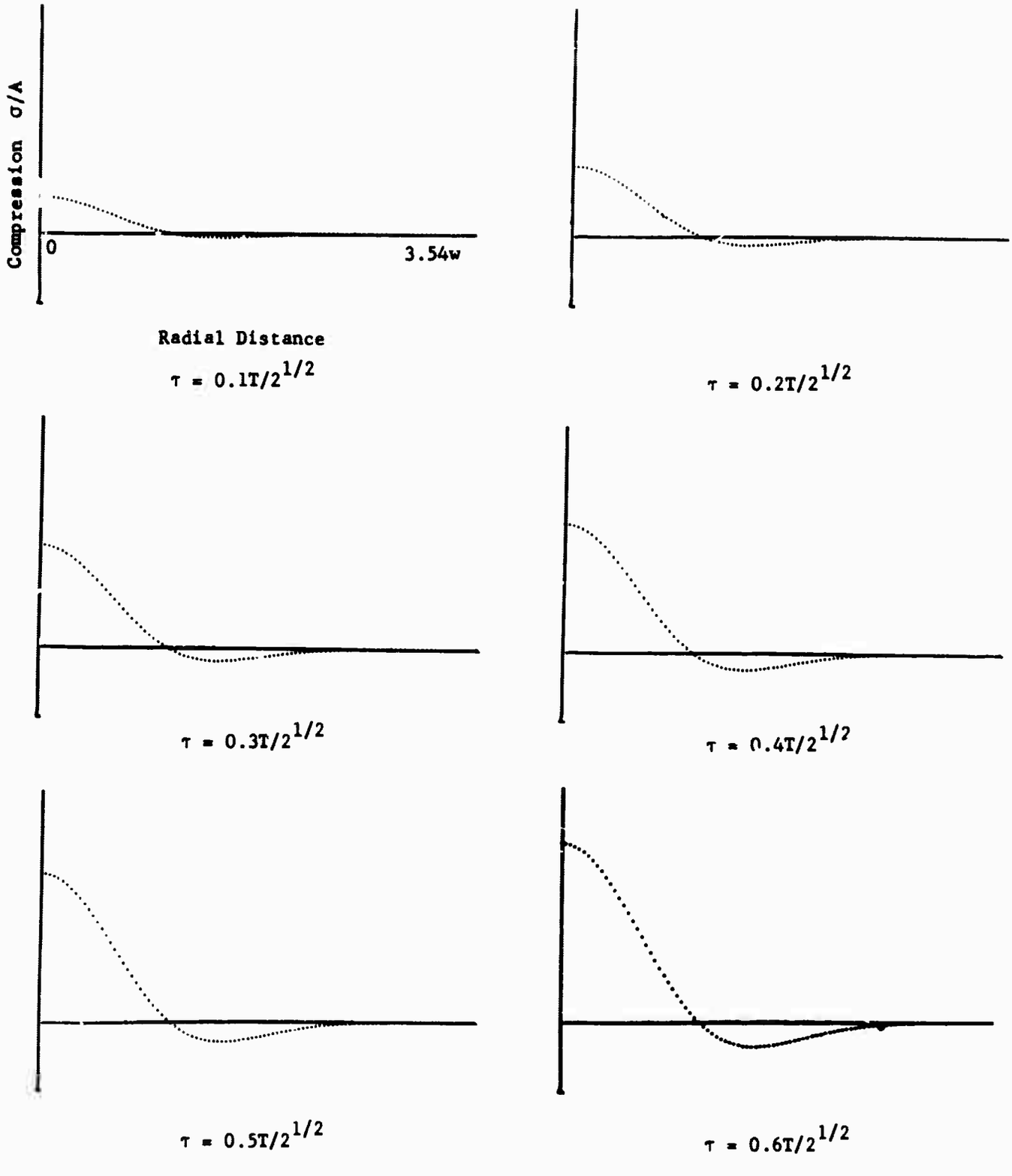

Figure 10. Sound Wave Compression at Various Times After an Initial Impulse

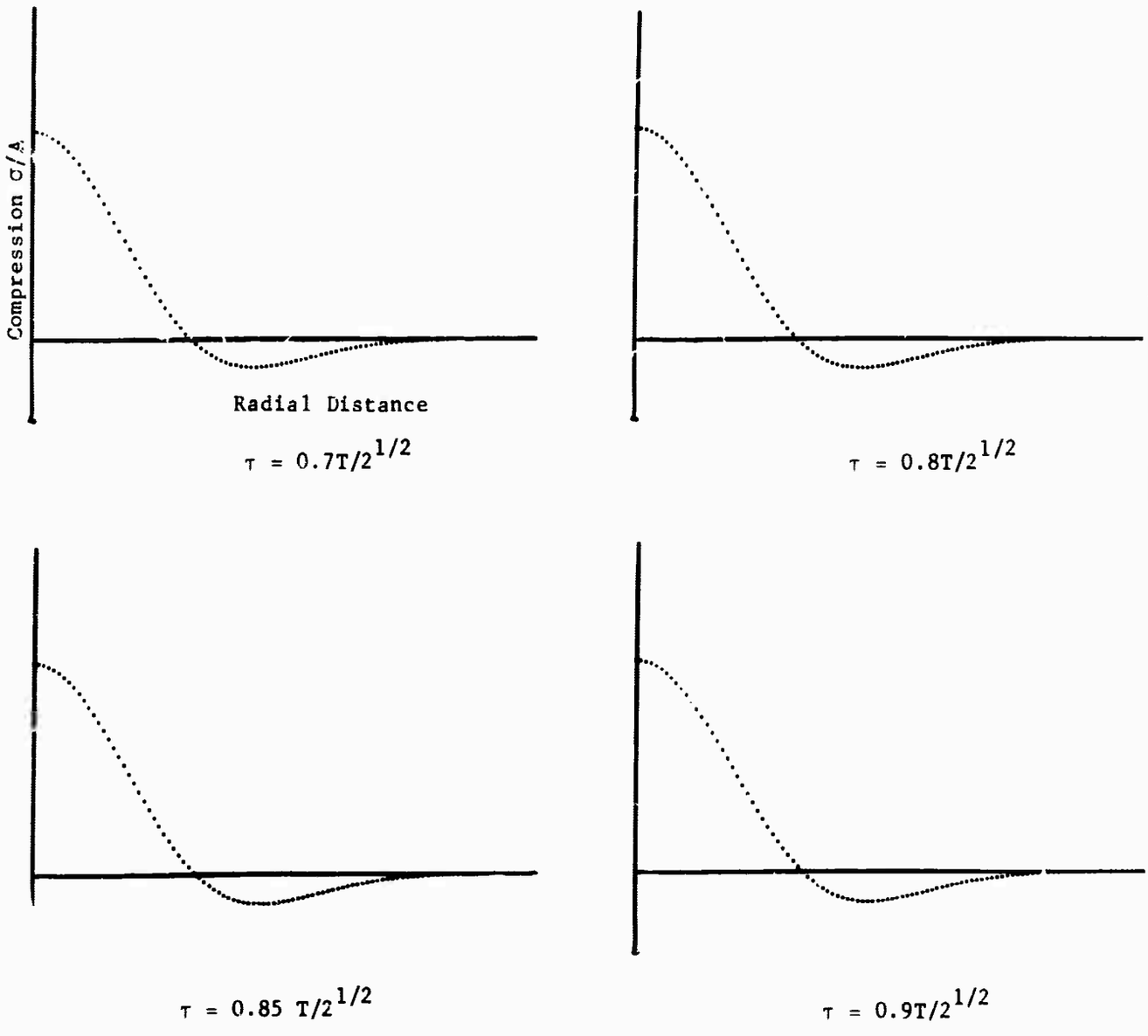

Figure 11. Sound Wave Compression at Various Times Near the First Peak

required axial Δn with the Δn due to the acoustic wave.

$$W_{TRAP} = \frac{9c\lambda^2}{4\pi} \left[\frac{n_o \rho_o}{(n_o^2 + 2)^2 (n_o^2 - 1)^2} \right] \frac{vw}{\sigma/A}$$

We may define the power for the impulse pair as

$$P = W/\Delta t = 3W/2p = \frac{W/T}{2p/3T}$$

and substitute $T = w/v$ so the trapping power becomes

$$P_{TRAP} = \frac{9c\lambda^2}{4\pi} \left[\frac{n_o \rho_o}{(n_o^2 + 2)^2 (n_o^2 - 1)^2} \right] \frac{v^2}{(2P/3T)(\sigma/A)}$$

The minimum trapping power will be required when the pulse half-time is such that $(2p/3T)(\sigma/A)$ is a maximum. This maximum is .261, and it occurs when $p = 1.22T$

$$P_{MIN} = 8.64c\lambda^2 \, n_o \, \rho_o \, v^2 / \left[\pi (n_o^2 + 2)^2 (n_o^2 - 1)^2 \right]$$

This minimum power depends only on the material properties and the wavelength. The beam size must be matched to the pulse half-time as follows:

$$p = 1.22T = 1.22 \, w/v$$

$$w_{matched} = .82 \, pv$$

For values of $p/T \ll 1$, $\sigma/A \cong 2p/3T$.

Hence in the limit of short pulses or large beams,

P_{TRAP} varies as w^2/p^2.

3.8 NUMERICAL CALCULATIONS

The acoustic trapping threshold curve for a material can be obtained with simple calculations. It is only necessary to obtain the sound velocity, the beam size that matches the pulse half-time, and the minimum power level. Then simple graphical methods yield the threshold curve.

Sound Velocity: The relevant sound velocity is that for a radially propagating compressional wave. For solids, use equation (1) in Section 3.4. The Young's modulus, density, and Poisson's ratio for glasses are found in the newer Schott glass catalogs.

Example: For BK-7, $Y = 8310\ kp/mm^2$, $\rho = 2.51\ g/cm^3$, $\epsilon = 0.208$. Multiply ρ by 10^3 to obtain the density in kilograms per cubic meter, and Y by 9.81×10^6 to obtain newtons per square meter from kiloponds per square millimeter. Hence $v = 4.27 \times 10^3$ meters per second.

Matched Beam Size: Let the pulse half-time p be measured at the half-peak points. Then $w_{matched} = .82\ pv$.

Minimum Power Level The minimum power level for the material is

$$P_{MIN} = (8.64c\lambda^2/\pi)\ \rho v^2 n_o / \left[(n_o^2 + 2)^2 (n_o^2 - 1)^2 \right]$$

Example: For BK-7, at $\lambda = 694.3$ nm, $n_o = 1.45$. The critical power level is 365 kilowatts.

Plotting the Threshold: Use log-log graph paper having equal size divisions for the horizontal and vertical scales. Draw a horizontal line corresponding to the minimum power level. Mark the matched point on the minimum power line, corresponding to the matched beam size.

For a quick, conservative overestimate of the trapping threshold curve, simply draw a line with a slope of 2 upward from the matched point. (The angle is 63.5° to the horizontal.)

For an accurate graph, plot the curve in Table I on a second piece of log-log paper. Lay the first piece over the second so the axes are parallel and the matched point is just over the bottom point on the second graph. Trace the curve.

TABLE I

NUMERICAL VALUES USEFUL FOR
PLOTTING ACOUSTIC TRAPPING THRESHOLD CURVES

Horizontal Axis	Vertical Axis
0.91	0.965
1.00	1.00
1.10	1.05
1.25	1.20
1.43	1.43
1.68	1.78
2.00	2.36
2.50	3.48
3.33	5.90
5.00	12.8
10.0	55.0

SECTION IV

AN ANALYTICAL SOLUTION OF THE LASER BEAM RADIUS EQUATION FOR KERR EFFECT TRAPPING

A high intensity laser beam passing through a material medium can focus itself into a long, thin filament and propagate without normal diffraction spreading. This self-trapping phenomenon arises when the medium's refractive index n is higher along the beam axis than along the beam edges. Such refractive index distribution acts like a series of thin positive lenses, as shown in Figure 12.

The high intensity beam can set up a focusing refractive index distribution by several physical mechanisms, such as electrostriction, anomalous dispersion, and reorientation of molecular dipole moments. The last effect is Kerr effect, after its discoverer, John Kerr (1824-1907). In liquids the molecular reorientation can occur in times on the order of 10 picoseconds. The effect is thus virtually instantaneous compared with the duration of nanosecond laser pulses, but it is much too slow to follow 500 terahertz light wave fields. The local change in index of refraction is proportional to the local beam intensity. When the beam power is above a certain threshold power level, the laser beam focuses itself to a smaller beam size and higher intensity. The smaller, higher intensity beam causes still stronger self-focusing until the beam has trapped itself at a small radius, limited by diffraction.

4.1 THE BEAM RADIUS EQUATION

This note sets forth an analysis of Kerr effect trapping. The analysis is based on a ray tracing equation published by Tien, Gordon, and Whinnery (Ref. 6). Equation (9) in that article reduces to

$$\partial^2 a/\partial z^2 = a^{-3} (\lambda/2\pi n_o)^2 + (a/n_o)\partial^2 n(0,z,t)/\partial r^2 \qquad (2)$$

Figure 12. Equivalent Beam Guides. The equivalence may be seen by integrating the optical path length (n dz) along the axes and along the edges of both figures. In both there is more retardation on axis than off.

where

$a(z,t)$ = beam radius to the point where the intensity is 1/e of the peak intensity,

$n(r,z,t)$ = local index of refraction

n_o = undisturbed or nominal index of the medium

λ = vacuum wavelength of the laser beam,

r,z = cylindrical coordinates for the beam.

For this equation to be valid Tien, Gordon, and Whinnery require that

1) "the light beam is...launched with a Laguerre-Gaussian or Hermite-Gaussian field distribution"
2) "the refractive index of the medium varies slowly in space (negligibly in an optical wavelength)"
3) the variations in n are small compared with n_o

The last two restrictions are violated when the beam is trapped to a filament with approximately one wavelength radius, and the scattered light is spread over a wide wavelength range. However, the equation can be used to study the collapse of the beam toward the trapped condition, and to study the phenomenon when the beam power is below threshold.

4.2 BEAM PROPAGATION WITHOUT SELF-FOCUSING

When the beam intensity is weak, the last term in equation (2) is negligible. The ray paths are then hyperbolas. The beam radius solution is

$$a(z) = \left[(a_o + a_1 z)^2 + (\lambda z/2\pi n_o a_o)^2\right]^{1/2} \qquad (3)$$

where a_o and a_1 are, respectively, the initial radius and initial slope of the rays just after entering the medium at $z = 0$. For example, let $\lambda = 1\mu m$, $n_o = 1.5$, $a_o = 0.1mm$, $a_1 = -0.001839$. Then the beam is focused to a radius of 0.05mm at $z = 4.1cm$. This is the case of a very gently focused beam. The

first frame of Figure 14 shows a plot of a(z) for this case . Note that the vertical, radius scale is greatly exaggerated.

4.3 THE LASER BEAM INTENSITY EQUATION

The lowest order mode for the laser beam has a nearly Gaussian intensity profile characterized by the radius, a, to the point where the intensity drops to 1/e of the peak intensity. If the propagation medium is not too violently inhomogeneous and if the inhomogeneity is radially symmetrical, the Gaussian profile is maintained along the beam, although the beam radius varies because of diffraction and focusing by the inhomogeneities.

The laser power may also vary as a function of time. For Q-switched pulse lasers generally the pulse energy can be measured and some rough idea of the time distribution of the pulse can be obtained. For purposes of analysis we can use a simple pulse shape such as the unit quartic pulse shown in Figure 13. This shape has a continuous derivative and finite extent.

Thus the laser beam intensity is

$$I(r,z,t) = (W/\pi a^2) \exp(-r^2/a^2)\, q(t;p)$$

where W is the pulse energy and q(t;p) is the unit quartic pulse of time constant p:

$$q(t;p) = \begin{cases} (15/16p)\,(t/p)^2(2-t/p)^2, & 0 \le t \le 2p \\ 0 & \text{otherwise.} \end{cases}$$

Of course, a is a(z,t) given by the solution of equation (2). The intensity distribution is so normalized that

$$\int_0^{2\pi} d\theta \int_0^{\infty} r\, dr \int_{-\infty}^{\infty} dt\, I(r,z,t) = W$$

independent of the value of z.

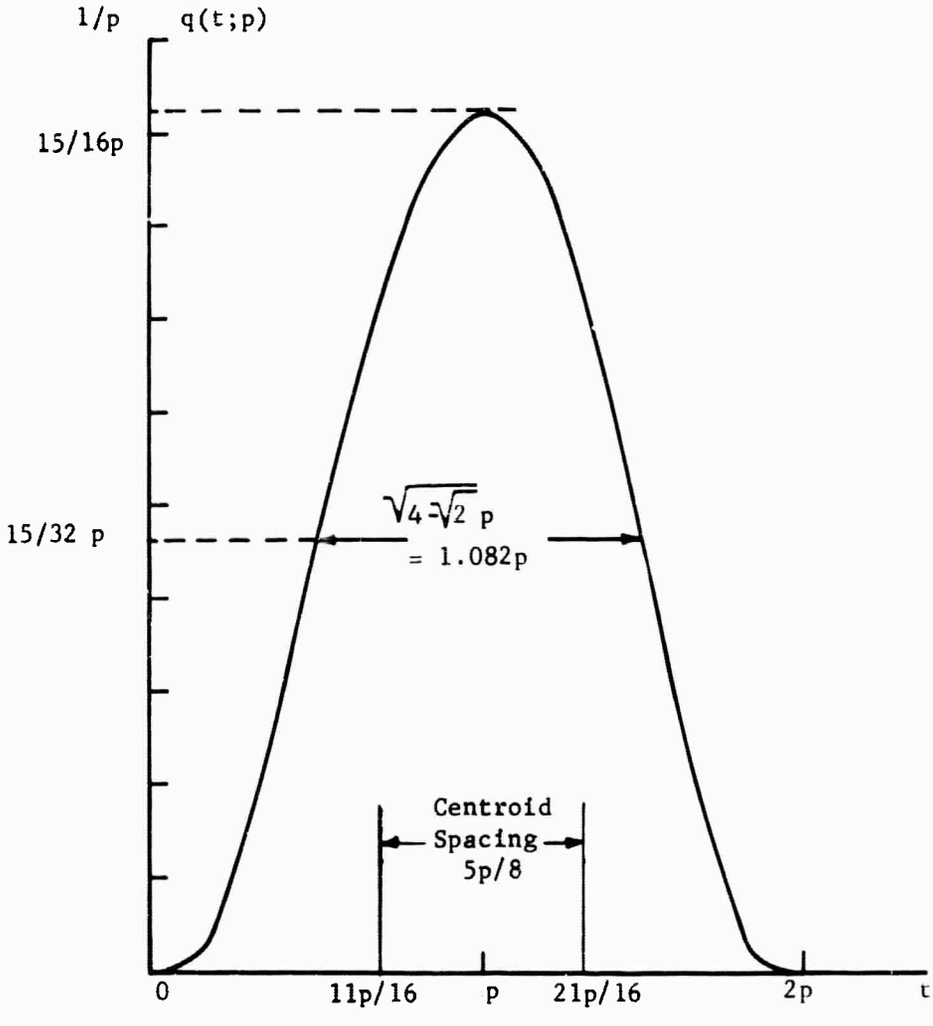

$$q(t;p) = \begin{cases} (15/16p)\ (t/p)^2(2-t/p)^2 & \text{for } 0 \le t \le 2p \\ 0 & \text{otherwise} \end{cases}$$

$$\int_{-\infty}^{\infty} q(t;p)\ dt = 1$$

Figure 13. Unit Quartic Pulse

4.4 VARIATION OF REFRACTIVE INDEX WITH INTENSITY

The change in refractive index can be expressed in cgs units as

$$n = n + \frac{2}{3}\lambda JE^2 + \cdots\cdots$$

where J is the high frequency Kerr constant due to molecular rotation. Thus the change in index is proportional to the local intensity for either a plane polarized or circularly polarized beam (although the constants of proportionality differ for the two cases). Let the constant of proportionality be K, depending on the wavelength, the material, and the beam polarization.

$$n(r,z,t) = n_o + KI\ (r,z,t)$$

In equation (2) the last term becomes

$$-a^{-3}(2\ KW/\pi n_o)\ q\ (t;p)$$

Since both terms on the right of equation (2) are proportional to a^{-3}, the solution at any time will be a hyperbola whose value and slope at $z = 0$ are a_o and a_1, respectively. However, the focal point and semiaxes of the hyperbola may vary with time. The equation becomes

$$\partial^2 a/\partial z^2 = f(t)a^{-3}$$

where

$$f(t) = (\lambda/2\pi n_o)^2 - 2KWq(t;p)/\pi n_o.$$

The solution is

$$a(z,t) = \left[(a_o + a_1 z)^2 + f(t)\ a_o^{-2}\ z^2\right]^{1/2}$$

A negative, zero or complex value of a would be a non-physical solution. This places a restriction on the minimum value of f(t) which occurs when $t = p$. We have $a^2(z,p)$ equal to a quadratic expression in z. In order that $a^2(z,p)$ be greater than zero for all real values of z, the discriminant of the quadratic expression must be negative. Then the only zeros of a^2 will

be complex. This condition implies that f(t) must always be positive. The minimum value of f(t) occurs when t=p, i.e., at the peak of the laser pulse. For a valid solution we must have

$$\Delta n/n_o < \frac{1}{2} (\lambda/2\pi n_o a)^2$$

where Δn, the on-axis increase in refractive index, is

$$\Delta n = KWq(p;p)/\pi a^2$$

This condition is equivalent to the Pierce stability criterion $L/f < 4$, where L and f are the spacing and focal length of lenses in a sequence (Ref. 5).

The threshold value of KW/p becomes $(KW/p)_{threshold} = 2\lambda^2/\pi n_o$

Let k be the fraction

$$k = (KW/p)/(KW/p)_{threshold}$$

Then f(t) becomes

$$f(t) = (\lambda/2\pi n_o)^2 [1-kq(t;p)/q(p;p)]$$

Refer to Figures 14 through 16 for plots of the beam radius when k = 0.999, 0.95, and 0.85.

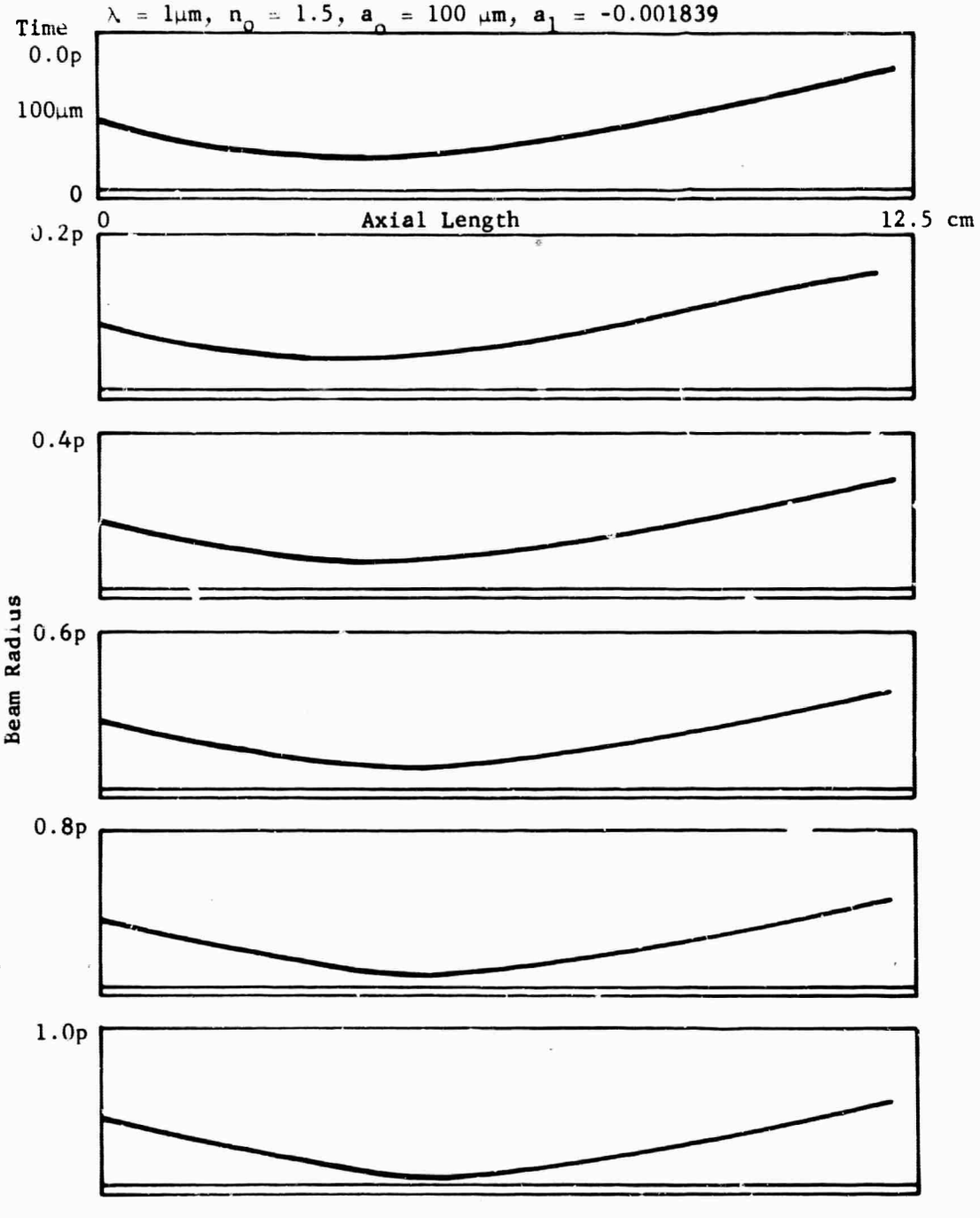

Figure 14. Kerr Effect Trapping at 99 Percent Threshold

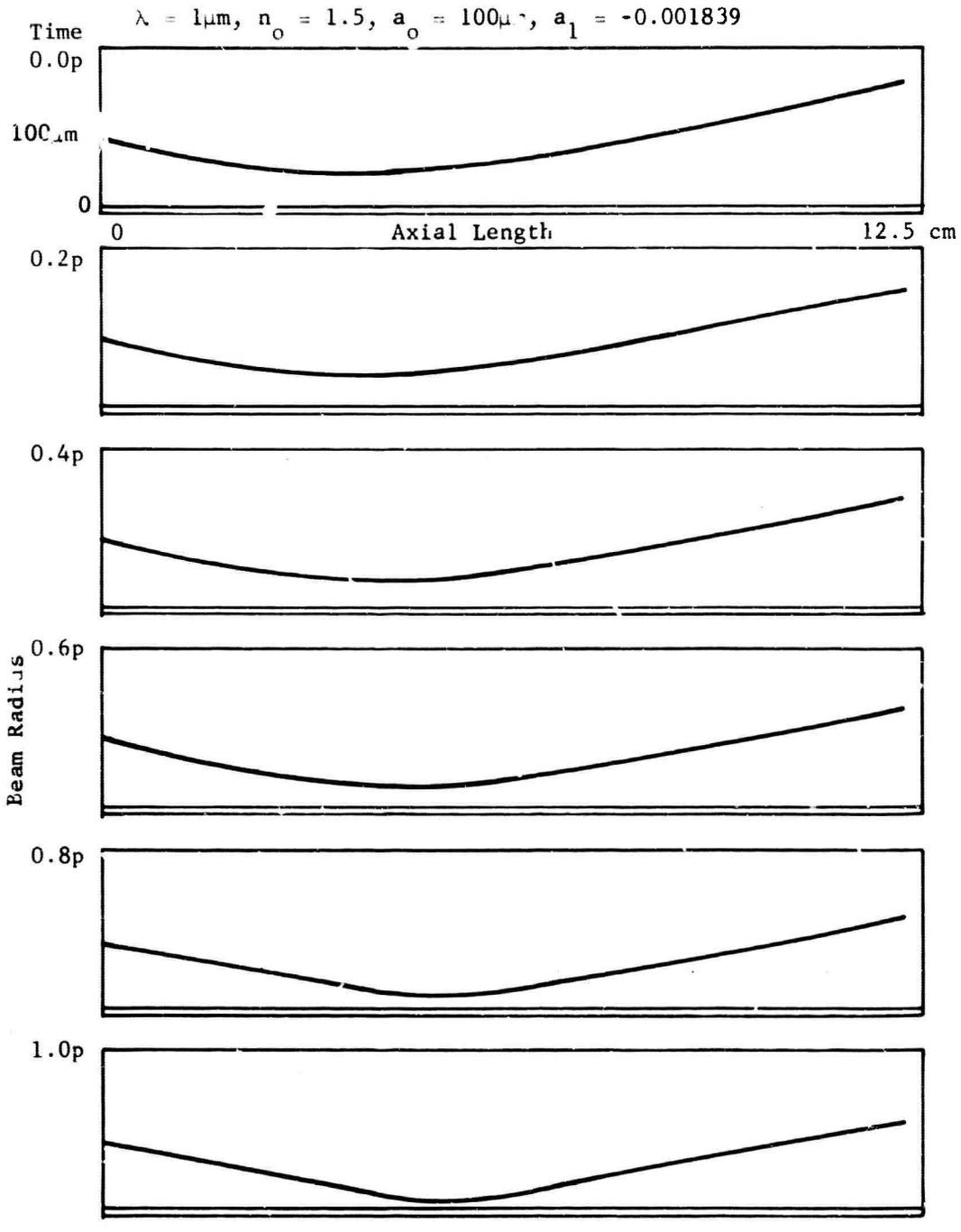

Figure 15. Kerr Effect Trapping at 95 Percent Threshold

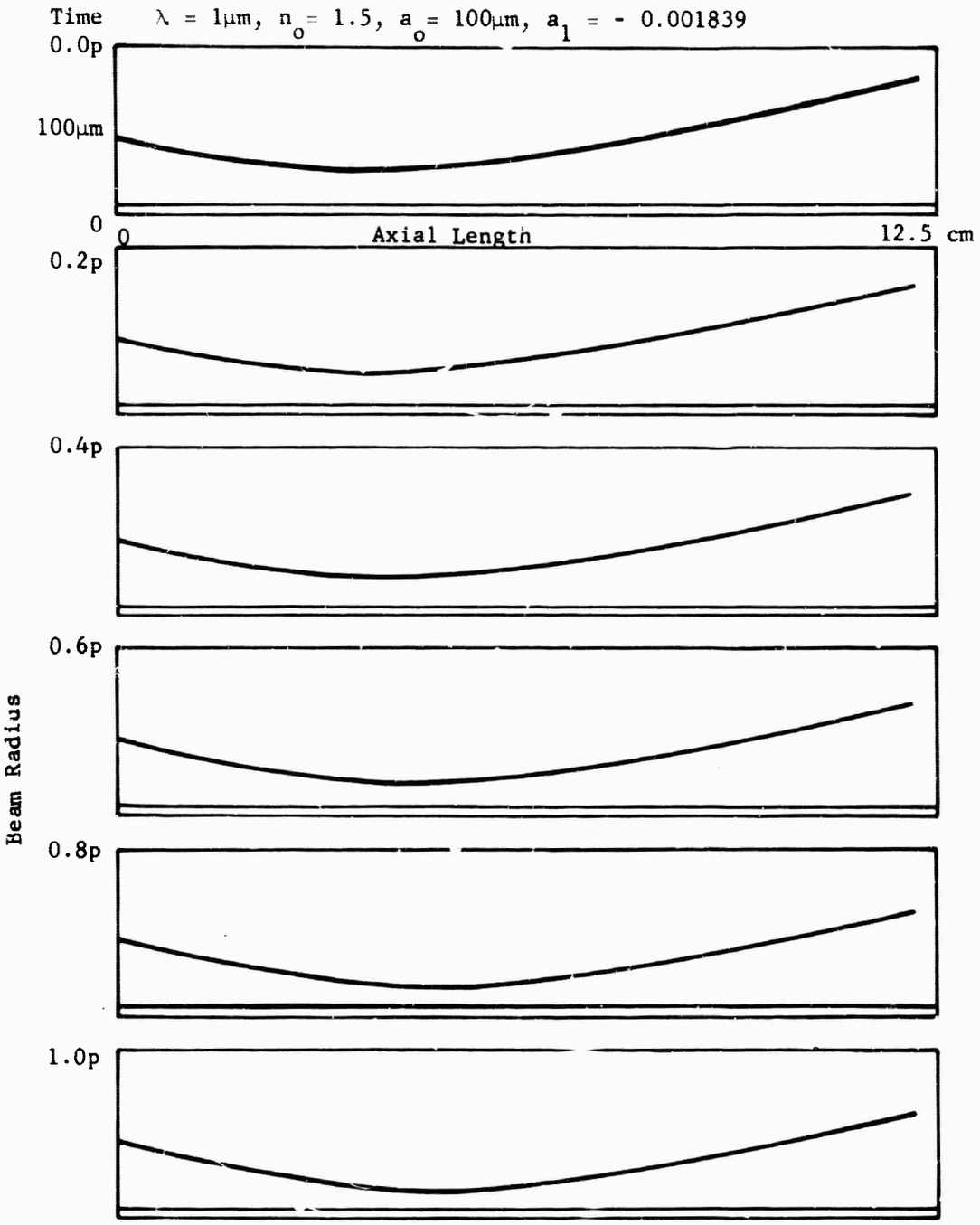

Figure 16. Kerr Effect Trapping at 85 Percent Threshold

SECTION V

BEAM TRACING IN THE ACOUSTIC TRAP

The theory, developed from the two-impulse model in Sections II and III, yields a threshold for acoustic beam trapping which is below the experimental damage thresholds for the glassy materials tested. It was solved by completely analytical means, using tabulated properties of special functions. The computer was only used to obtain values for the radial sound wave off the axis of the beam. That computation was not essential to the solution, although it did give the following important insight: The refractive index distribution set up by the acoustic wave is initially a focusing distribution, although its strength varies with time. However, the theory did not allow for the continuous interaction of light and sound, nor did it show how the focusing action develops with time.

5.1 OTHER FEATURES OF THE GLASS DAMAGE PHENOMENON

A complete theory should also explain the other observed features of internal, filamentary glass damage, such as the following:

1) The Spectrum of the Side-Scattered Light
   A white light flash is seen when the damage event occurs. Ruby laser light may be shifted from 6943Å down to 4000Å. Such large shifts can only be explained by a very strong dynamic refractive index change.

2) Starting Location of the Damage Track
   Even if the laser is focused at the entrance face of the glass sample, the damage track never begins at the entrance face. There is always a short interval between the entrance face of the sample and the start of the track.

3) Exit Face Pitting

Usually the track ends in a pit on the exit face of the glass sample. As a matter of fact, the threshold for the exit face pitting appears to be a little lower than the threshold for track formation. Nevertheless, the phenomena is different from the type of surface damage reported by others.

4) Location of Damage Stars

The damage track is not always continuous; it may start and stop several times in the sample. Often there is a damage star on the upstream end of the track. These damage stars are localized regions of gross fracture. Occasionally they show discoloration, indicating possible chemical decomposition. If the damage track extends upstream of the damage star it usually only does so for a very short distance compared to the extension downstream from the damage star. The location of the damage star is intriguing. If the damage starts in the damage star and then propagates downstream to form the track, why doesn't the damage star cast a downstream shadow and prevent the beam from concentrating in the thin filament?

5) Track Propagation Speed

Since the damage event occurs in nanoseconds, its dynamics are difficult to follow. There is experimental evidence that the event that forms the track propagates at about 10 times the speed of sound in the glass. The experimental evidence does not show unequivocally that the propagation is either upstream or downstream.

Most of these features are explained qualitatively in the theory of electrostrictively driven acoustic beam trapping.

5.2 DEFINITION OF THE PROBLEM

Our purpose is to understand how the acoustic beam trap forms, not how the damage occurs. Therefore we only need consider small acoustic pressure changes in the material. We will see how these lead to a beam instability when the power exceeds a certain threshold. The nature of the instability is such that the beam rapidly focuses itself into a thin filament. The damage occurs when the beam is in this trapped condition. The instability itself can be studied by means of a geometric ray tracing equation which includes first order diffraction effects. This beam tracing equation is equation (2) of Section IV.

The sound wave satisfies essentially the same conditions as those given in Section III, except that it is driven continuously by the light wave, rather than running inertially after an impulse. For a gently focused beam, axial components of the sound wave field are negligible in comparison with the radial components.

The desired solution will show a graph of the beam radius plotted versus axial length for each of many small time intervals during the laser pulse. The time distribution of the laser pulse can be assumed to be the quartic pulse distribution described in Section IV, since the actual details of the shape of the laser pulse do not have too much bearing on the threshold for damage and on the time development of the beam trap.

5.3 THE COUPLED EQUATIONS

The sound wave equation is

$$\partial^2\sigma/\partial r^2 + r^{-1}\partial\sigma/\partial r + \partial^2\sigma/\partial z^2 = v^{-2}\,\partial^2\sigma/\partial t^2 - (1/6vn_o\rho_o)(n_o^2+2)(n_o^2-1)(W/\pi)q(t;p) \cdot 4a^{-4}(1-r^2/a^2)\exp(-r^2/a^2)$$

The beam tracing equation is

$$\partial^2 a/\partial z^2 = a^{-3}(\lambda/2\pi n_o)^2 + (a/6n_o^2)(n_o^2+2)(n_o^2-1)\,\partial^2\sigma(o,z,t)/\partial r^2$$

The general solution of these coupled, nonlinear, partial differential equations has been left as an exercise for the computer. One simplification can be made immediately. The beam tracing equation involves only the second derivative with respect to r of the on-axis sound wave solution. Since the sound wave equation is linear we may take its Hankel transform analytically. When z is held fixed, the Hankel transform of σ satisfies an ordinary differential equation in t. This ordinary equation may be solved using initial values of the Hankel transform, and of its derivative with respect to time, and assuming a step-plus-ramp driving function. The solution is then found by taking the inverse Hankel transform. Since the beam tracing equation involves only the second derivative of the sound wave amplitude at $r = 0$, and the inverse Hankel transform involves r only as part of the argument of the zeroth-order Bessel function, we may perform the differentiation analytically under the integral sign. Thus for each time step and each value of z, the sound wave equation can be solved with only one numerical integration. The use of a step-plus-ramp driving function allows us to take a much coarser time step than we would require if we used an impulsively driven equation.

5.4 THE STEP-BY-STEP COMPUTER SOLUTION

The problem is divided up into sections and slices as shown in Figure 17. In its present state of development the computer program can handle 101 sections. The zeroth section is the entrance face of the solid or liquid medium. The initial beam radius and entrance angle are fixed on the zeroth section. Since the solution is radially symmetrical, it will be the same in each radial slice.

The computer program must store values of a for each of the 101 sections. Also for each section, it must store 40 values of the Hankel transform of the sound wave, and 40 values of the derivative of the Hankel transform of the sound wave with respect to time. An array of 101 points is also set aside for the second derivative of the sound wave with respect to r. No Bessel function storage or Bessel function subprogram is required. Initially the Hankel transform of the sound wave and its derivative with respect to time

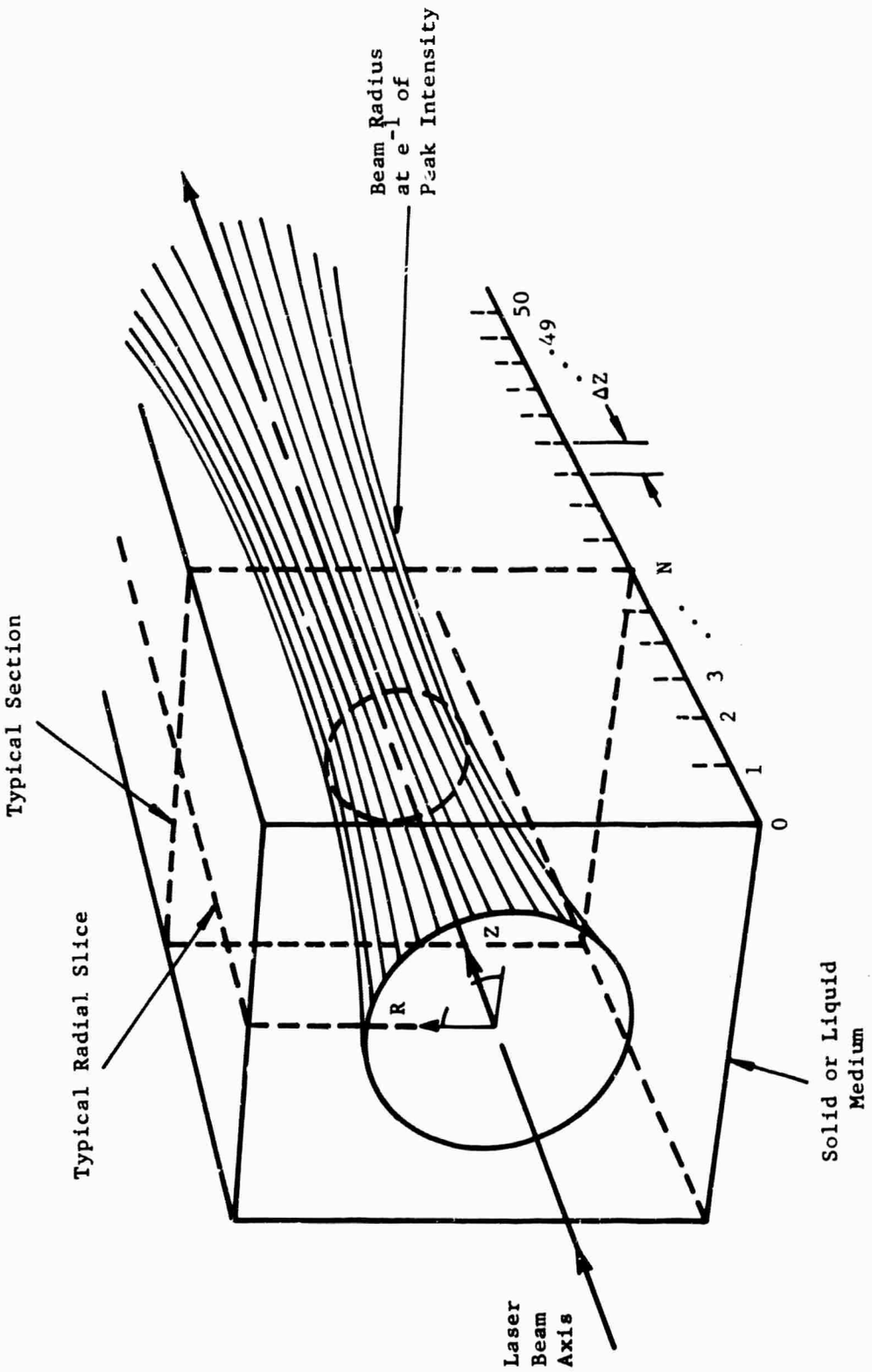

Figure 17 . Geometry of the Beam Trapping Analysis

are set to zero along with the second derivative of the sound wave with respect to r. The solution then proceeds in steps:

1) Solve the beam tracing equation using the Runge-Kutta method. The axial step size in the solution is 1/5 of the interval between sections. Values of the second derivative of the sound wave with respect to r are interpolated by Lagrange cubic fitting.

2) Store 101 values of the beam radius a. Also save these values on tape for later plotting.

3) If the time has not yet reached 2.0p, the end of the laser pulse, advance the time by a small time step and obtain the new value of the beam power at that time.

4) For each section of the beam compute the second derivative of the sound wave with respect to r by using Simpson intergration. At the same time revise the value of the Hankel transform of the sound wave and its time derivative for the next time step.

5) Go to 1.

The program parameters are the wavelength, the nominal refractive index, the initial beam radius and the initial slope of the beam radius at the entrance face, and the fraction of pulse power divided by theoretical threshold.

5.5 TYPICAL RESULTS FOR ACOUSTIC BEAM TRAPPING

Figure 18 depicts acoustic beam trapping when the pulse power is 300% of the threshold. There are 11 frames showing the beam radius plotted versus axial length for 11 different times during the pulse. The first frame shows the path of the beam when the illumination has just begun. The sixth frame gives the trace when the pulse power is highest. The 11th frame shows the path taken by the light in the trailing end of the pulse.

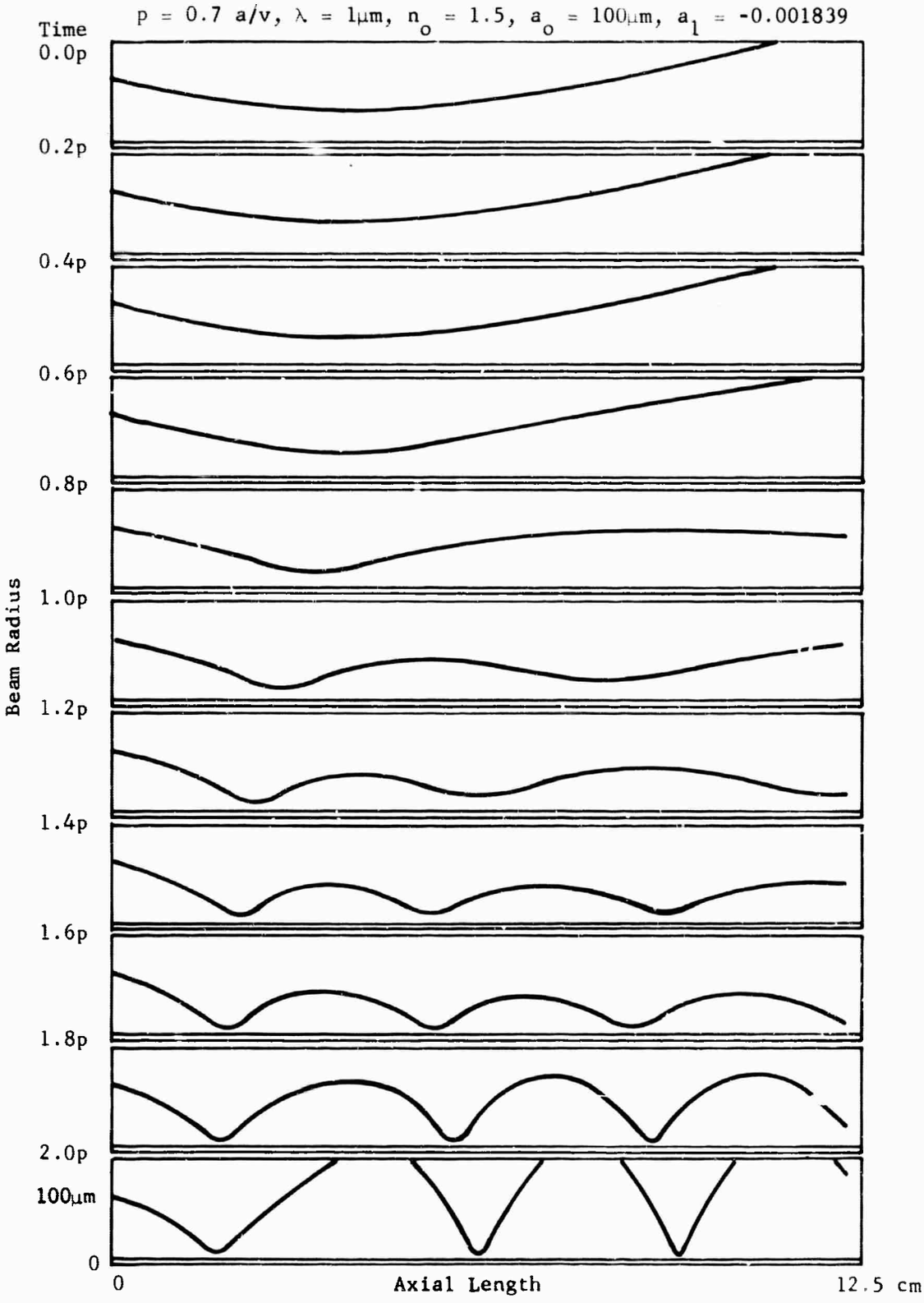

Figure 18. Acoustic Beam Trapping at 300 Percent Threshold

The action may be interpreted by considering that each section of the beam forms an acoustic lens. Initially the lenses have zero power, but some of them build up focusing power faster than others. The strongest lens is formed at the focus of the beam. As its focusing power builds up in time it causes the beam to be refocused at some distance downstream. As the strength of the acoustic lens continues to build up, its focal length is shortened so the second focus moves upstream. The second focus likewise forms a third focus and so on. A little after the laser pulse is half over, three definite foci have appeared in the 12-1/2cm region plotted. At the same time that these acoustic lenses are becoming stronger because of the inertial properties of the material, the laser pulse power is decreasing. The net result is regions of sharper and sharper focus interspersed by regions in which the beam radius is increasing. Eventually the beam will be able to escape again to large radii.

Note in the last frame that the sharpest focus occurs the farthest downstream. This is to be expected since the focus there is the result of two strong lenses upstream. Another important feature is the motion of the first focus. Notice how it moves upstream in the beam. This is because the acoustic lenses in the first few sections of the sample are also developing in strength with time.

Several features of the damage phenomenon are immediately explained. The fact that white light is scattered largely from the region of the damage stars is easily seen to follow from the fact that the highest focusing and therefore the highest index of refraction occur at places that become damage stars. Also the track propagates backward, becoming more and more sharply defined until it ends in a damage star. If there are more than one, the damage stars occur in backward sequence. The farthest downstream occurs first, then the next one upstream, then finally the damage star closest to the upstream end of the beam. Thus, the damage event does not cast a shadow that gets in its own way.

The reason why it is difficult to measure the speed of propagation of the damage event is now apparent. The intensity varies widely and more than one focus region may move past the velocity-sensing optics.

The pit on the exit face of the glass sample is formed by axial sound wave components which do become large when the beam is sharply focused. There can never be a damage pit on the entrance face. The entrance conditions of the beam are fixed; therefore, the beam cannot focus itself sharply at the entrance face of the glass.

All of the qualitative features of the phenomenon are a sharp contrast to the phenomenon of Kerr effect trapping, in which there is one focus region that moves downstream.

BLANK PAGE

SECTION VI

DERIVATIONS

A number of derivations are presented in this section. Each one is the analytical solution of some part of the model for acoustic laser beam trapping. In many cases the results were evaluated by computer programs. In those cases, an outline of the program and typical plots are given.

6.1 RADIAL ACOUSTIC WAVES UNDER IMPULSE EXCITATION AND UNDER CONTINUOUS DRIVING FORCES

The crude (but useful) model of Section III divides the laser pulse into two impulses. The first impulse excites an acoustic wave. By the time of the second impulse the acoustic wave has set up an inhomogeneous refractive index distribution. If the distribution is sufficiently converging, the light beam from the second impulse will be trapped at a small radius.

The value of the model lies in the fact that the sound and light equations are decoupled. The light acts only once, instantaneously, on the material. The resulting sound wave reacts only once, instantaneously, on the light beam. Although this model does not represent the actual phenomenon very realistically, it is relatively easy to analyze and it does give good values for the trapping threshold.

The model can be improved slightly by computing the sound wave response to a continuous driving force applied by the light for the duration of the laser pulse. In that case, the sound wave, as it develops, should focus the beam. To treat the focusing problem, however, it would be necessary to calculate the radial sound wave in many cross sections of the beam. An alternative is to consider the case where the light pulse is so weak that the acoustic waves do not focus the beam significantly. It is then still possible to compare the acoustic response to a continuous driving force with the impulse response.

When we made the calculation, we found that the response was basically the same. There was a phase delay due to the later arrival of the majority

of the light energy, and the amplitude of the response was reduced slightly as the pulse half-time increased. Nevertheless, the same initial focusing distribution followed by an outward propagating ripple and slow settling of the wake was observed. These results increase our confidence in the validity of the two-impulse model of Section III.

The Sound Wave Equation:

Let σ be the acoustic compression, and r be the radius in cylindrical coordinates. The radial sound wave equation becomes

$$\partial^2\sigma/\partial r^2 + r^{-1}\partial\sigma/\partial r = \partial^2\sigma/\partial t^2 - (A + Bt)(1 - r^2)\exp(-r^2)$$

where the driving term has the Laplacian of a Gaussian radial distribution (as before) and a step-plus-ramp temporal distribution. (The general pulse temporal distribution may be approximated to any desired degree of accuracy by a continuous series of steps and ramps.) The equation is Hankel transformed by multiplying it by $rJ_o(r)$ and integrating from 0 to ∞. In general, the Hankel transform of the Laguerre polynomial is

$$\int_0^\infty \exp(-r^2)L_n(r^2)\, rJ_o(\rho r)dr = (1/2n!)\,(\rho/2)^{2n}\exp(-\rho^2/4)$$

Our transform has $L_1(r^2) = 1 - r^2$, so the transformed equation becomes

$$\partial^2\bar{\sigma}/\partial t^2 + \rho^2\bar{\sigma} = (A + Bt)\,\rho^2\exp(-\rho^2/4)/8$$

where

$$\bar{\sigma}(\rho,t) = \int_0^\infty \sigma(r,t)r\, J_o(\rho r)dr$$

is the Hankel transform of the compression and

$$\int_0^\infty (r\partial^2\sigma/\partial r^2 + \partial\sigma/\partial r)\, J_o(\rho r)dr = -\rho^2\bar{\sigma}$$

is a known transformation. (See Ref. 7).

The transformed equation is just the one-dimensional wave equation with a step-plus-ramp driving term. This forced equation is easily solved by Laplace transforms. (It could even be solved for a unit quartic pulse forcing

term. That solution, however, would not be particularly useful later in the general problem of acoustic focusing.) The solution for the Hankel transform of the compression is

$$\bar{\sigma}(\rho,t) = \bar{\sigma}(\rho,0)\cos\rho t + [\partial\bar{\sigma}(\rho,0)/\partial t]\,\rho^{-1}\sin\rho t$$

$$-[A(\cos\rho t-1) + B\rho^{-1}(\sin\rho t-\rho t)]\exp(-\rho^2/4)/8$$

given the initial "position" $\bar{\sigma}(\rho,0)$ and "velocity" $[\partial\bar{\sigma}(\rho,0)/\partial t]$ of the compression.

In order to evaluate the acoustic response to a driving function of arbitrary temporal distribution by a continuous step-plus-ramp approximation, it is necessary to have the "velocity" as a function of time also. Then the "position" and "velocity" at the end of the timestep become the new initial "position" and "velocity" for the next timestep. The velocity is obtained by simple differentiation:

$$\partial\bar{\sigma}(\rho,t)/\partial t = -\bar{\sigma}(\rho,0)\,\rho\sin\rho t + [\partial\bar{\sigma}(\rho,0)/\partial t]\cos\rho t$$

$$-[-A\rho\sin\rho t + B(\cos\rho t-1)]\exp(-\rho^2/4)/8$$

Integral Representation of the Sound Wave Solution:

The acoustic compression is now obtained by the inverse Hankel transform.

$$\sigma(r,t) = \int_0^\infty \bar{\sigma}(\rho,t)\,\rho J_0(\rho r)\,d\rho$$

$$= \int_0^\infty \{\bar{\sigma}(\rho,0)\,\rho\cos\rho t + [\partial\bar{\sigma}(\rho,0)/\partial t]\sin\rho t$$

$$-[A\rho(\cos\rho t-1) + B(\sin\rho t-\rho t)]\exp(-\rho^2/4)/8\}\,J_0(\rho r)\,d\rho$$

We note that the term $\bar{\sigma}(\rho,0)$ is multiplied by ρ in the integral. Thus, if $\bar{\sigma}\rho$ is always evaluated, rather than $\bar{\sigma}$ alone, there will be no division by zero at $\rho=0$.

Before the start of the optical pulse at t=0, the medium is at rest. Thus, $\sigma(r,0) = \bar{\sigma}(\rho,0) = 0$. In the case of an extremely short optical pulse there may be an initial velocity at t=0, as in Section III. The initial velocity due to an impulse of Gaussian spatially distributed light is

$$\partial\sigma(r,0)/\partial t = (1-r^2)\ \exp(-r^2)$$

with the Hankel transform

$$\partial\bar{\sigma}(\rho,0)/\partial t = \rho^2\ \exp(-\rho^2/4)/8$$

as before.

Method of Computation:

The integral representation of the sound wave solution above was checked by computing and displaying the wave. This computer check was important because the integral representation is a starting point for further reductions to the computing formulas used in the beam tracing program.

The only input variable for the computation is the pulse half-time, measured in units of the material time constant. Time runs from 0 through 10 material time constants in steps of 0.1 time constant. The unit quartic pulse starts from zero at T=0 and is evaluated after each timestep, for finite pulse half-times. If the pulse half-time is zero, the program computes and stores the initial velocity $\partial\bar{\sigma}(\rho,0)/\partial t$ as above.

For every pulse halftime entered, the program computes a movie of 101 frames. In each frame the wave amplitude is plotted at 21 points along the radius scale, from 0 to 5 beam radii. After computation the maximum amplitude range was found to be -0.05 to +0.34 for the impulse-excited wave, and less for other excitations. The frame consists of 23 words of 24 bits each. The first word contains the number of points, not counting the 0th point; it is 20 in this case. The next word contains the number of repetitions for the frame, equal to the ratio of the timestep for this frame to the shortest timestep in the movie. Since all the timesteps are equal in this program, the number of repetitions is 1 for each frame. The remaining 21 words contain the points packed for oscilloscope display. The leading 4 bits contain a code number 7, causing the oscilloscope to draw intensified vectors from the last point displayed to the new point. The next 10 bits specify the scaled value of the radius, and the 10 least significant bits are the scaled value of the amplitude. The words are written in BCD coding, 16 octal fields 8 characters wide, without spaces. A graph of every 4th frame was also printed as a quick check on the computation.

The Bessel function was computed according to a polynomial approximation (Ref. 4). For argument Z less than or equal to 3,

$$A = (Z/3)^2$$

$$J_o(Z) = 1 + A(a_o + A(a_1 + A(a_2 + A(a_3 + A(a_4 + Aa_5))))).$$

For larger arguments,

$$A = 3/Z$$

$$J_o(Z) = (b_o + A(b_1 + A(b_2 + A(b_3 + A(b_4 + A(b_5 + Ab_6)))))).$$

$$\cdot \cos(Z + c_o + A(c_1 + A(c_2 + A(c_3 + A(c_4 + A(c_5 + Ac_6)))))Z^{-1/2}$$

The coefficients are:

$a_o = -2.2499997$	$b_o = +0.79788456$	$c_o = -0.78539816$
$a_1 = +1.2656208$	$b_1 = -0.00000077$	$c_1 = -0.04166397$
$a_2 = -0.3163866$	$b_2 = -0.00552740$	$c_2 = -0.00003954$
$a_3 = +0.0444479$	$b_3 = -0.00009512$	$c_3 = +0.00262573$
$a_4 = -0.0039444$	$b_4 = +0.00137273$	$c_4 = -0.00054125$
$a_5 = +0.0002100$	$b_5 = -0.00072805$	$c_5 = -0.00029333$
	$b_6 = +0.00014476$	$c_6 = +0.00013558$

These formulas are supposed to give correct results to within $\pm 5 \times 10^{-8}$ absolute error.

At first we attempted to evaluate the integral representation with a 21-sample Simpson approximation. However, the solution did not vanish sufficiently as T approached 10. After the ripple passed out off the movie to the right and the wake settled, a low-spatial-frequency ripple seemed to move back toward the left. This is explained as insufficient cancellation by the sinpt and cospt terms, which have wavelengths of 0.628 at T=10. For a 21-sample Simpson approximation over the range 0 to 5 the sampling interval is 0.25, or 2.5 samples per wavelength. Therefore, we changed to a 41-sample Simpson approximation over the same range, taking 5 samples per wavelength, to achieve satisfactory results.

When we speak of a 41-sample Simpson approximation we are including the sample at zero, which does not contribute to the integral. Thus, in the entire movie 40 samples of the integral were taken to evaluate each of 21 points in each of 101 frames, 40 x 21 x 101 = 84,840 samples in all. Each sample requires a value of the Bessel function. To save running time, we set up a table of the 41 x 21 = 861 values of the Bessel function actually used. Let i be the index for r values, and let j be the index for ρ values. Then

$$r_i = 0.25i, \qquad i = 0,1,\ldots,20$$
$$\rho_j = 0.125j, \qquad j = 0,1,\ldots,40$$
$$J_{ij} = J_o(r_i\rho_j) = J_o(0.03125ij)$$

Clearly, $J_{ij} = J_{ji}$, and $J_{oj} = J_{io} = 1$, so the table contains many duplicate entries. However, we could not think of a simple indexing scheme to reduce the number of entries by eliminating redundancy, so we stored the entire table as it stands in computer memory at the start of the program. Various complicated indexing schemes are possible, of course, but none of the ones we thought of could be computed quickly.

Three additional working arrays are required to compute the integral. Each array has 41 elements. It is necessary to save the values of $\rho\bar{\sigma}(\rho, t = \text{timestep})$ and $\partial\bar{\sigma}(\rho,t=\text{timestep})/\partial t$ after each frame, in order to have $\rho\bar{\sigma}(\rho,0)$ and $\partial\bar{\sigma}(\rho,0)/\partial t$ for the next frame. Also, the kernel of the integral (apart from the factor $J_o(\rho r)$) does not involve r, so 41 samples of it may be saved and used repeatedly in each frame. It is useful to include the Simpson weighting coefficients as part of the kernel.

Finally, the 21 points in each frame were stored so that they could be written as a single record for each frame.

The program is carried out in steps as follows. Here the equal sign means place the value of the expression on the right into the cell named on the left.

1. Create the Bessel function table.
   $J_{ij} = J_o(ijd\rho dr)$, $i = 0,1,\ldots,20$; $j = 0,1,\ldots,40$
   where $d\rho = 1/8$ and $dr = 1/4$.

2. Read p, the half-time of the pulse. If there are no more values of p to read, stop.

3. Clear working arrays.

   $t = 0;\ \ h_j = k_j = 0,\ \ j = 0,1,\ldots,40$

   where t is the time, h_j is $\bar{\sigma}(\rho_j,0)$

   and k_j is the jth sample of the kernel.

4. Set the initial "velocity".

   $d_j = 0$ if the p is non-zero

   $d_j = \rho_j^2 \exp(-\rho_j^2/4)/8,\ j = 0,1,\ldots,40$ is p is zero

   where d_j is $\partial\bar{\sigma}(\rho_j,0)/\partial t$

5. Go to 9.

6. Compute the step and ramp coefficients.

   $a = q(t-dt;p),\ b = [q(t;p)-a]/dt$

   where q is the unit quartic pulse of Section IV, and dt is the timestep, 1/10.

7. Compute the kernel. Also, compute the values of "position" and "velocity" required for the next timestep.

   Do the next 6 replacements successively as j takes on the values 1,2,...,40.

   $e = \exp(-\rho_j^2/4)/8$

   $f = a\rho_j(\cos\rho_j dt - i) + b(\sin\rho_j dt - p_j dt)$

   $g = h_j\cos\rho_j dt + d_j\sin\rho_j dt - ef$

   $k_j = (1/3)\ d\rho\ 2(j \bmod 2+1)g$

   $d_j = -h_j\sin\rho_j dt + d_j\cos\rho_j dt - e[-a\rho_j\sin\rho_j dt + b(\cos\rho_j dt - 1)]$

   $h_j = g$

   Finally, adjust the end sample of the kernel.

   $k_{40} = k_{40}/2$

8. Compute the sound wave solution at 21 radial points. Simultaneously print them every 4th timestep.

$$s_i = \Sigma_{j=o}^{40} J_{ij} k_j, \quad i = 0,1,\ldots,40$$

9. Pack the points as described before into 21 words and write them on magnetic tape.

10. Take the next timestep. If this is the last frame, go to 2. Otherwise,
t = t + dt
and go to 6.

This 87-statement SDS Fortran IV program required 1 minute 54 seconds for compilation and 4 minutes 12 seconds to load and run four cases with ρ equal to 0, 0.5, 1, and 1.5. Later we used a second program to place corresponding frames of the four movies in four quadrants of a single frame of a new movie. The latter movie permitted us to make phase and amplitude comparisons for the four cases.

The results are plotted and reproduced in Figures 19 through 24, for t = 0 to t = 7.1. The upper left quadrant of each frame shows the response for p = 0, the upper left for p = 0.5, the lower left for p = 1, and the lower right for p = 1.5.

6.2 THE LOCAL LENS ESTABLISHED BY A SINGLE LASER IMPULSE

A laser pulse whose half-time was negligible compared with the material time constant would pass through a transparent dielectric on a hyperbolic path without being focused appreciably by electrostriction, because of the time required for acoustic compression. Nevertheless, the medium would be set into motion, and the focusing power would develop with time. An analysis of this model shows how a single impulse can set up a localized acoustic lens at the initial focus of the laser beam. Because the acoustic lens is localized, it can cause a second focus for the laser beam, provided that the next laser impulse comes before the sound wave has subsided. This behavior may be contrasted with the behavior in Kerr effect trapping, where only one focus would occur under such conditions.

The second term on the right-hand side of equation (2) of Section IV is the focusing term in the beam tracing equation,

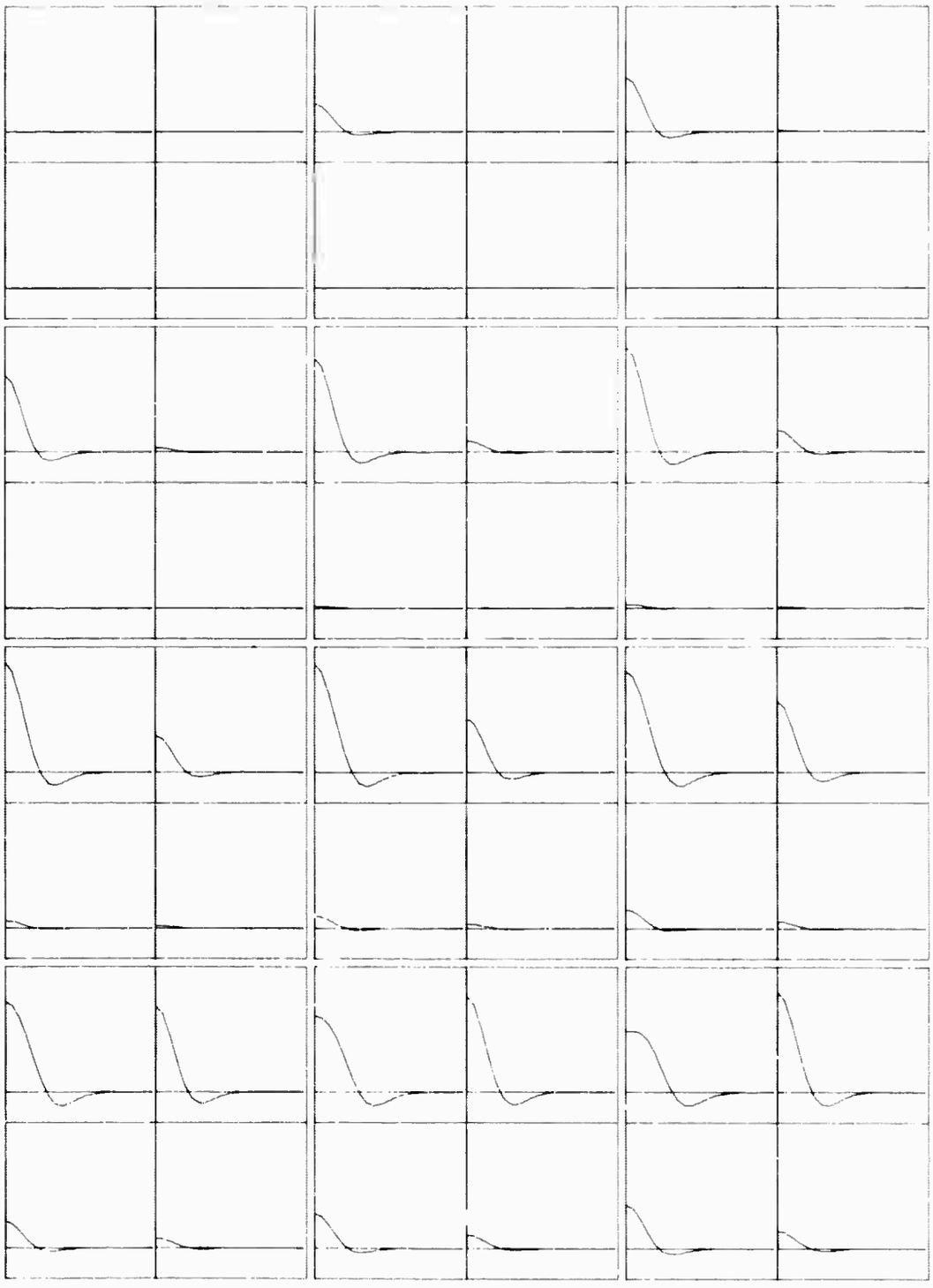

Figure 19. Amplitude Versus Radius For Four Sound Waves, T = 0.0 to 1.1

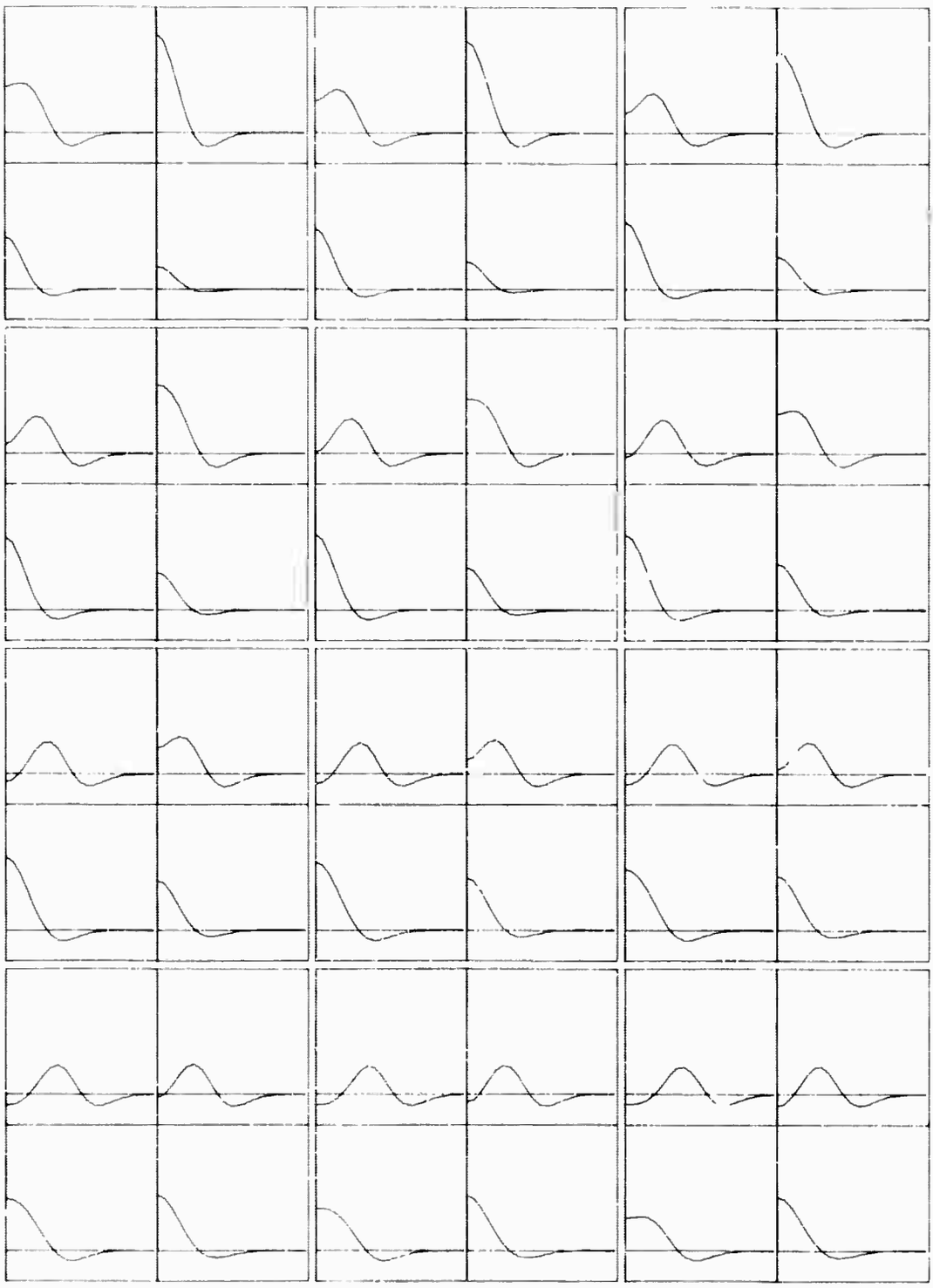

Figure 20. Amplitude Versus Radius For Four Sound Waves, T = 1.2 to 2.3

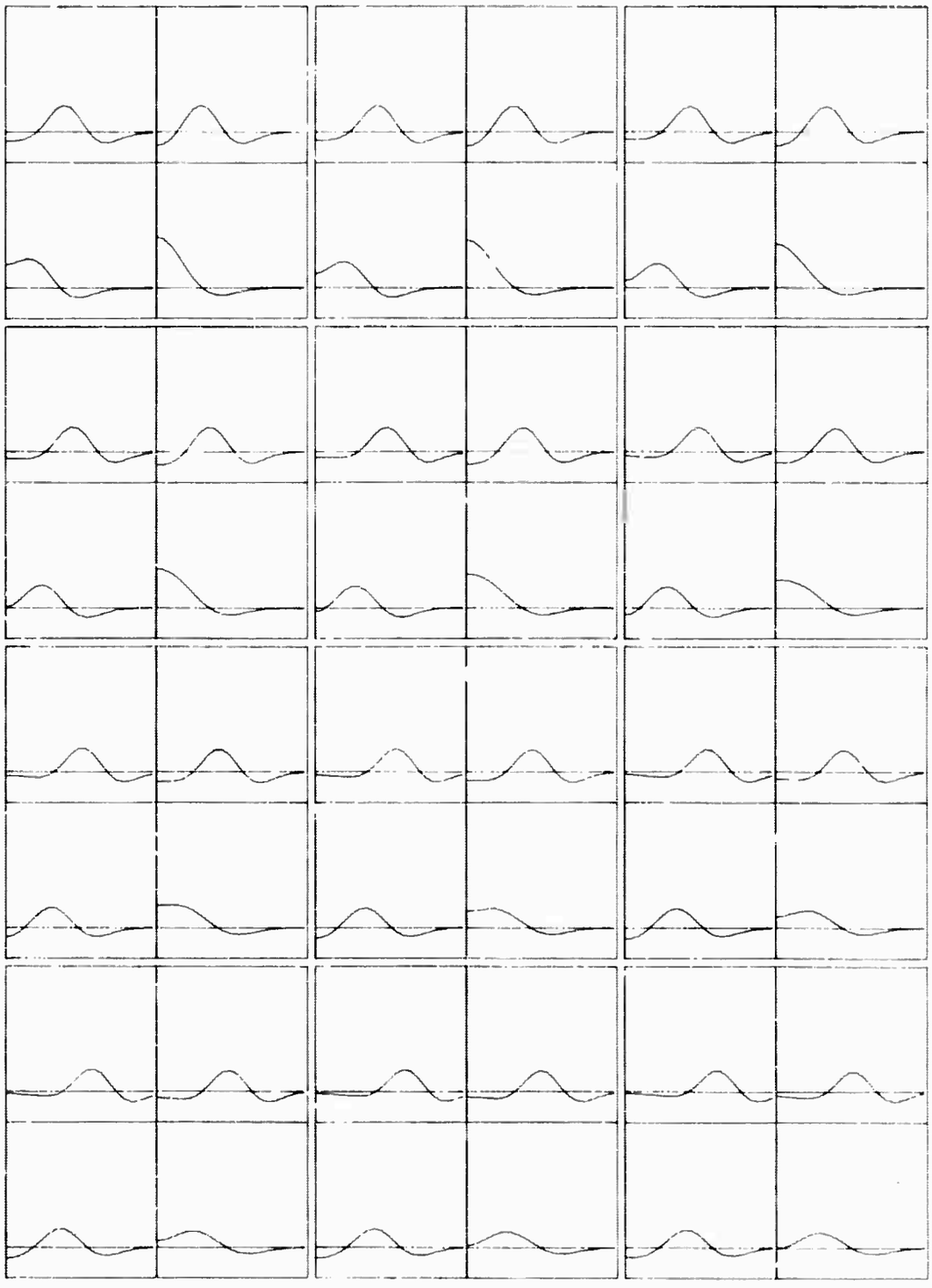

Figure 21. Amplitude Versus Radius For Four Sound Waves, T = 2.4 to 3.5

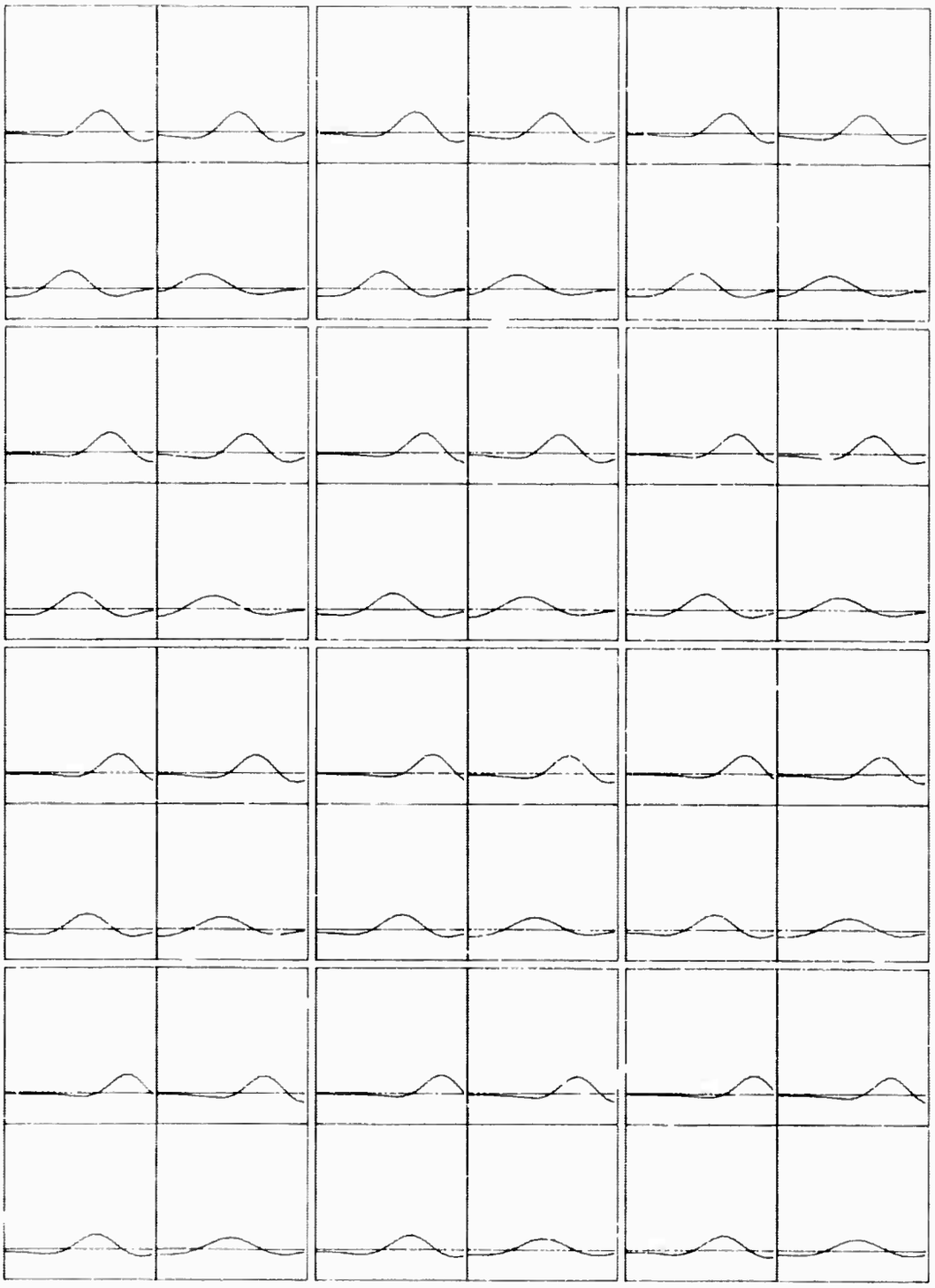

Figure 22. Amplitude Versus Radius For Four Sound Waves, T = 3.6 to 4.7

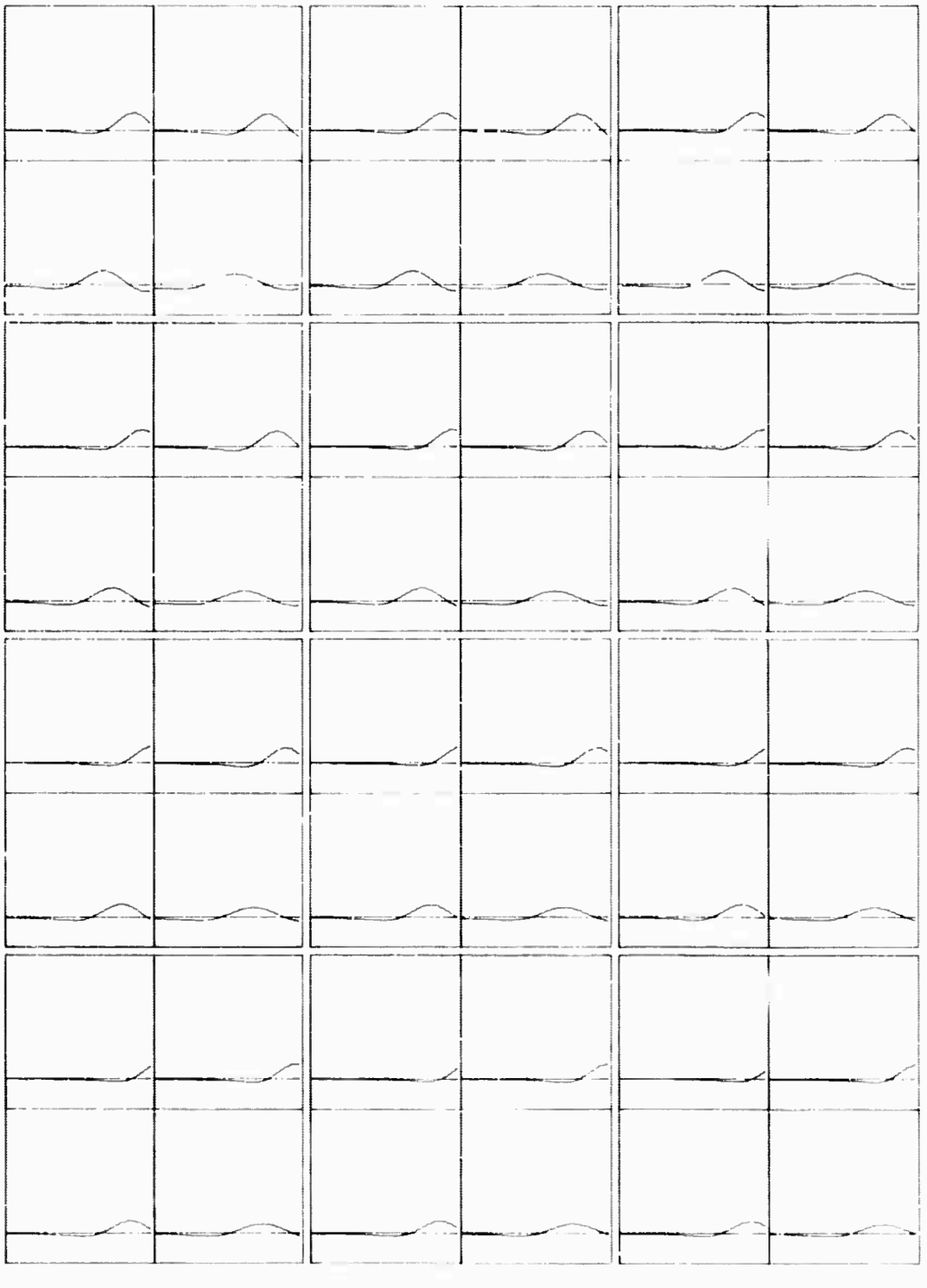

Figure 23. Amplitude Versus Radius For
Four Sound Waves, T = 4.7 to 5.9

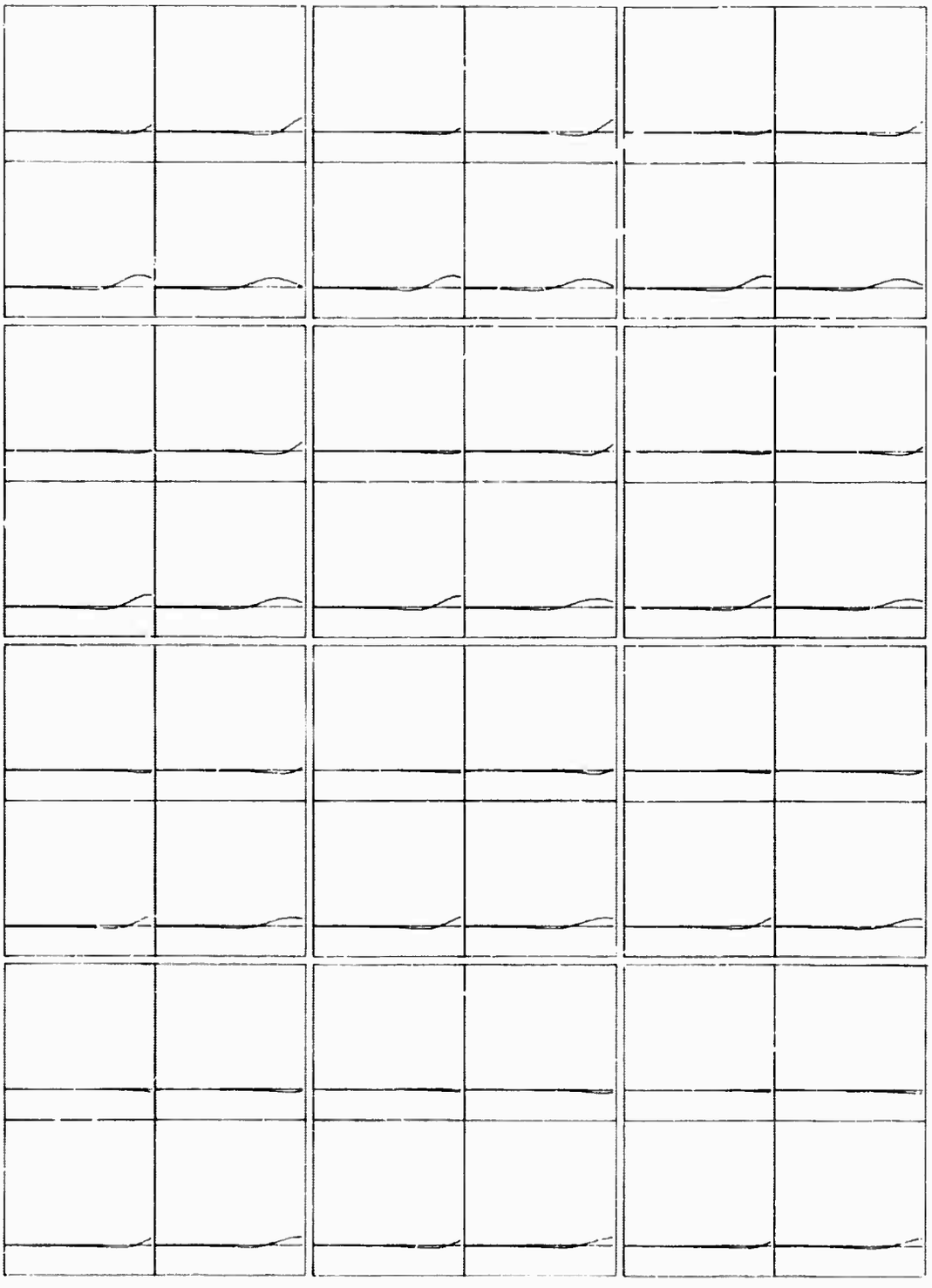

Figure 24. Amplitude Versus Radius For Four Sound Waves, T = 6.0 to 7.1

$$(a/n_o)\ \partial^2 n(0,z,t)/\partial r^2$$

Derivatives of the refractive index are proportional to the acoustic compression. These can be evaluated analytically at r = 0. The result will be the dependence of the focusing term on the initial hyperbolic beam radius.

We are therefore interested in the second derivative of the acoustic compression along the beam axis as a function of z and t. This quantity is proportional to the coefficient of the focusing term. We will use the integral representation of the compression when excited only by an initial impulse. To get the full dependence on beam radius, we will work the problem through in unscaled, physical coordinates.

The path taken by the beam through a homogeneous medium is

$$a(z) = \left[(a_o + a_1 z)^2 + (\lambda z/2\pi n_o a_o)^2\right]^{1/2}$$

as in equation (3), Section IV. The laser beam intensity is

$$I(r,z,t) = (W/\pi a^2)\ \exp(-r^2/a^2)\ [\delta(t) + \delta(t-5p/8)]/2$$

where the spacing 5p/8 between delta functions corresponds to placing an impulse at the centroid of each half of the unit quartic pulse.

The force exerted on the medium by electrostriction, assuming the Clausius - Mosotti relation applies, is

$$\vec{f} = (n_o^2 + 2)\ (n_o^2 - 1)\ \vec{\nabla}\ I/3n_o c$$

The velocity field after the first impulse is

$$\int_{-\infty}^{o+} \vec{f}\ dt = g\ \dot{\vec{u}}\ (r,z,0^+)$$

where g is the average density of the medium, by conservation of linear momentum, and the compression is the negative divergence of the displacement,

$$\sigma = -\ \vec{\nabla} \cdot \vec{u}$$

Thus, in cylindrical coordinates, taking the time derivative of the above equation,

$$\partial\sigma(r,z,0+)/\partial t = -\vec{\nabla}\cdot\dot{\vec{u}}\,(r,z,0+)$$

$$= -(n_o^2+2)(n_o^2-1)\,\nabla^2\int_{-\infty}^{0+} I\,dt/3\,n_o cg$$

$$= -[W(n_o^2+2)(n_o^2-1)/6n_o cg\pi a^2]$$

$$\left\{r^{-1}\,\partial[r\partial\,\exp(-r^2/a^2)/\partial r]/\partial r\right\}$$

$$= (2W/3\pi\,n_o cga^4)\,(n_o^2+2)\,(n_o^2-1)\,(1-r^2/a^2)\exp(-r^2/a^2)$$

The Hankel transform is easily evaluated as

$$\partial\bar{\sigma}(\rho,z,0+)/\partial t = (2W/3\pi n_o cga^2)\,(n_o^2+2)\,(n_o^2-1)\cdot$$

$$\int_0^\infty (r/a)\,J_o[(a\rho)(r/a)]\,(1-r^2/a^2)\,\exp(-r^2/a^2)\,d(r/a)$$

$$= (W/12\,\pi\,n_o cg)\,(n_o^2+2)\,(n_o^2-1)\,\rho^2\,\exp(-a^2\rho^2/4)$$

The material was in a state of rest before the initial impulse, so $\bar{\sigma}(\rho,z,0+) = 0$. Also, there is no forcing term after the impulse, as the intensity drops to zero again, so A = B = 0. Thus, by substitution in the integral representation of the solution we obtain

$$\sigma(r,z,t) = \int_0^\infty [\partial\bar{\sigma}(\rho,z,0+)/\partial t]\,\sin(\rho vt)\,J_o\,(\rho r)\,d\rho$$

$$= C\int_0^\infty \rho^2\exp(-a^2\rho^2/4)\,\sin(\rho vt)\,J_o(\rho r)\,d\rho$$

where we have inserted the velocity of sound v and

$$C = (W/12\pi n_o cgv)\,(n_o^2+2)\,(n_o^2-1)$$

We may now obtain $\partial^2\sigma(0,x,t)/\partial r^2$ by differentiating under the integral sign. We have

$$\partial^2 J_o(\rho r)/\partial r^2 = [J_2(\rho r) - J_o(\rho r)]\,\rho^2/2$$

and

$$J_2(0) = 0,\quad J_o(0) = 1.$$

This leads to

$$\partial^2\sigma(0,z,t)/\partial r^2 = -(C/2)\int_0^\infty \rho^4 \exp(-a^2\rho^2/4)\sin(\rho vt)\,d\rho$$

The remaining integral is just a Fourier transform. A useful property of Fourier transforms permits us to simplify the integral further. If

$$F(y) = \int_0^\infty f(x)\sin(xy)\,dx \quad \text{for } y > 0$$

is the Fourier transform of $f(x)$, then the Fourier transform of $x^{2m} f(x)$ is $(-1)^m\, d^{2m} F(y)/dy^{2m}$. Thus we need only evaluate

$$K = \int_0^\infty \exp(-a^2\rho^2/4)\sin(\rho vt)\,d\rho = \mathrm{Im}\left[\int_0^\infty \exp(-a^2\rho^2/4 + i\rho vt)\,d\rho\right]$$

where Im[ ] denotes the imaginary part. By completing the square in the exponential and shifting the variable we can reduce the remaining part of the integral to a finite interval.

$$K = \mathrm{Im}\left\{\int_0^\infty \exp\left[-(a\rho/2 - ivt/a)^2\right] d\rho\, \exp(-v^2t^2/a^2)\right\}$$

Let $\xi = a\rho/2 - ivt/a$; then

$$K = \mathrm{Im}\left\{(2/a)\exp(-v^2t^2/a^2)\int_{-ivt/a}^\infty \exp(-\xi^2)\,d\xi\right\}$$

$$= \mathrm{Im}\left\{(2/a)\exp(-v^2t^2/a^2)\left[\int_0^\infty \exp(-\xi^2)\,d\xi - \int_0^{-ivt/a} \exp(-\xi^2)\,d\xi\right]\right\}$$

Now let $\eta = -\xi/i$ and take only the imaginary part

$$K = (2/a)\exp(-v^2t^2/a^2)\int_0^{vt/a} \exp(\eta^2)\,d\eta$$

With the above result, the focusing term becomes

$$\partial^2\sigma(0,z,t)/\partial r^2 = -(C/2)\,d^4K/d(vt)^4$$

It is now convenient to change to scaled coordinates. We let $\tau = vt/a$ so

$$\partial^2\sigma(0,z,t)/\partial r^2 = -Ca^{-5}d^4\left[\exp(-\tau^2)\int_0^\tau \exp(\eta^2)d\eta\right]/d\tau^4$$

$$= -Ca^{-5}\left[20\tau - 8\tau^3 + (12 - 48\tau^2 + 16\tau^4)\exp(-\tau^2)\int_0^\tau \exp(\eta^2)d\eta\right]$$

For very small values of τ we may replace the exponentials by 1 and drop all terms of order τ^2 or less.

Then,

$$\partial^2\sigma(0,z,t \ll a/v)/\partial r^2 \cong -8Ca^{-5}\tau = -8Cvt\ a^{-6}$$

As the terms in higher powers of τ become dominant, the coefficient of the focusing term becomes even more localized near the original focus.

The Dawson integral $D(\tau) = \exp(-\tau^2)\int_0^\tau \exp(\eta^2)d\eta$ is tabulated (Ref. 4, p. 319). For reference, other derivatives are as follows:

$$dD/d\tau = 1 - 2\tau D$$
$$d^2D/d\tau^2 = -2\tau + (4\tau^2 - 2)D$$
$$d^3D/d\tau^3 = 4\tau^2 - 4 + (12\tau - 8\tau^3)D$$
$$d^4D/d\tau^4 = 20\tau - 8\tau^3 + (12 - 48\tau^2 + 16\tau^4)D$$

An asymptotic expansion for D is

$$\text{Lim } D(\tau \to \infty) = -i\exp(-\tau^2)\sqrt{\pi}/2 + (1/2\tau)\left[1 + 1/2\tau^2 + 1\cdot 3/(2\tau^2)^2 + 1\cdot 3\cdot 5/(2\tau^2)^3 + \ldots\right]$$

Each of the derivatives of D becomes 0 as τ approaches infinity because the polynomial terms are cancelled by subtraction. Thus, the formulas are mathematically correct, but inconvenient for computation for large values of τ.

The coefficient of the focusing term was computed and plotted versus z in Figure 25. The function of a was given by equation (3) of Section IV, plotted in the first frame of Figure 14. In Figure 25, reading left to right and top to bottom, we see the local development of the focusing coefficient as τ runs from 0 to 2. In the two-impulse model of trapping, the second

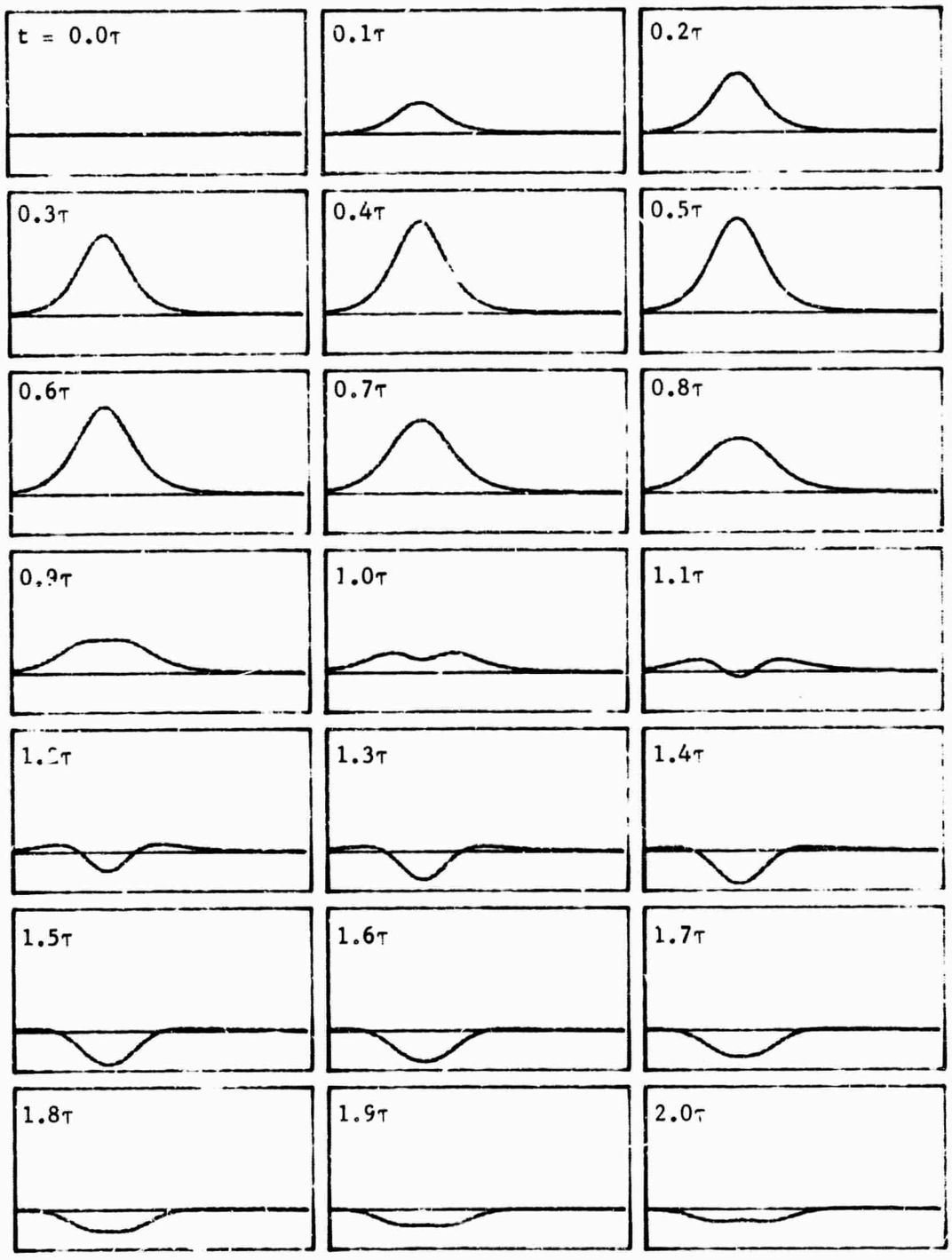

Figure 25. Coefficient of the Focusing Term Plotted Versus Axial Length At Various Fractions of the Material Time Constant, After an Initial Impulse

impulse could arrive anytime before $\tau = 1.2$ and still pass through a converging acoustic lens. If the pulse half-time were much longer, it would first be focused, then defocused.

In the plot the coefficient at the initial focus appears to develop with a phase just twice as fast as the coefficient at the left-hand edge, and the amplitude is 32 times greater. This is because of the 2 to 1 ratio of values of a.

The Dawson integral was computed by running Simpson integration, using a step size of 0.0005. (A step size of 0.05 was too large for stable computation beyond about $\tau = 4$.)

Let

$$d_j = \int_0^{0.001j} \exp(\eta^2)d\eta$$

Then

$$d_o = 0$$

$$t = 0.001j \quad d_j = d_{j-1} + (0.0005/3)\left\{\exp[(t-0.001)^2] + 4\exp[(t-0.0005)^2] + \exp(t^2)\right\}$$

defines the running Simpson integral used.

6.3 STEP-BY-STEP SOLUTION OF THE COUPLED EQUATIONS

The solution of the coupled sound and beam radius equations has already been discussed in Section V. The actual formulas used by the computer program will be presented here.

The step-plus-ramp driven sound wave solution required becomes

$$\partial^2\sigma(0,z,t)/\partial r^2 = -(1/2)\int_0^\infty \rho^2\left\{\bar{\sigma}(\rho,z,0)\rho\cos\rho t + [\partial\bar{\sigma}(\rho,z,0)/\partial t]\sin\rho t - (a^2/8)\exp(-a^2\rho^2/4)\left[A a\rho(\cos a\rho t - 1) + B(\sin a\rho t - a\rho t)\right]\right\}d\rho$$

$$\bar{\sigma}(\rho,z,t)\rho = \bar{\sigma}(\rho,z,0,\rho\cos\rho t + [\partial\bar{\sigma}(\rho,z,0)/\partial t]\sin\rho t - (a^2/8)\exp(-a^2\rho^2/4)[A a\rho(\cos a\rho t - 1) + B(\sin a\rho t - a\rho t)]$$

$$\partial\bar{\sigma}(\rho,z,t)/\partial t = -\bar{\sigma}(\rho,z,0)\rho \sin \rho t + [\partial\bar{\sigma}(\rho,z,0)/\partial t] \cos \rho t$$

$$-(a^2/8) \exp(-a^2\rho^2/4)[-Aa\rho \sin a\rho t + B(\cos a\rho t - 1)]$$

These may be evaluated by Simpson integration as described before in Subsection 6.1. The equations now include a = a(z,t), which is obtained by beam tracing before each timestep. The coefficient of electrostriction can be entered separately, because the sound wave equation is linear.

For the Runge-Kutta solution of the beam tracing equation it was necessary to interpolate between points where the focusing term was known. We used the Lagrange cubic fitting formula. If interpolation is required between X_n and X_{n+1}, where Y_{n-1}, Y_n, Y_{n+1}, Y_{n+2} are known ordinates for equally spaced abscissas, and $\xi = (X-X_n)/h$ is the fraction of the distance from the last abscissa to the point of interpolation divided by the step size,

then,

$$Y(X_n + \xi h) = -\xi(\xi-1)(\xi-2)\, Y_{n-1}/6 + (\xi^2-1)(\xi-2)\, Y_n/2$$

$$-\xi(\xi+1)(\xi-2)\, Y_{n+1}/2 + \xi(\xi^2-1)\, Y_{n+2}/6$$

See Ref. 4, pp. 878f.

REFERENCES

[1] R.Y. Chiao, E. Garmire, and C.H. Townes, "Self Trapping of Optical Beams," Phys. Rev. Letters 13, 15 (October 12, 1964), pp 479-482.

[2] G.N. Steinberg, J.G. Atwood, P.H. Lee and S.A. Ward, Research into the Causes of Laser Damage to Optical Components: Final Report, the Perkin-Elmer Corporation TR-7945, February 28, 1965. Prepared for US Army Electronics Command AMSEL-HL-L, Fort Monmouth. Contract #DA28043 AMC 00009.

[3] Julius Adams Stratton, Electromagnetic Theory, McGraw-Hill (1941) p.140.

[4] Milton Abramowitz and Irene A. Stegun, Handbook of Mathematical Functions with Formulas, Graphs, and Mathematical Tables, National Bureau of Standards, Appl. Mathematics Series No. 55, U.S. Government Printing Office, Washington, D.C., June 1964.

[5] J.R. Pierce, Theory and Design of Electron Beams, D. Van Nostrand, 2nd ed. (1954), p. 195.

[6] P.K. Tien, J.P. Gordon, and J.R. Whinnery, "Focusing of a Light Beam of Gaussian Field Distribution in Continuous and Periodic Lens-Like Media," Proceedings of the IEEE, 53, No. 2 (February 1965), pp 129-136.

[7] Ian A. Sneddon, Fourier Transforms, McGraw-Hill (1951), pp 125-128.

DOCUMENT CONTROL DATA - R&D

(Security classification of title, body of abstract and indexing annotation must be entered when the overall report is classified)

1. ORIGINATING ACTIVITY *(Corporate author)*
The Perkin-Elmer Corporation
Norwalk, Connecticut

2a. REPORT SECURITY CLASSIFICATION
Unclassified

2b. GROUP

3. REPORT TITLE

Acoustic Self-Trapping of Laser Beams

4. DESCRIPTIVE NOTES *(Type of report and inclusive dates)*
Final Report

5. AUTHOR(S) *(Last name, first name, initial)*
Kerr, Edwin L.

6. REPORT DATE	7a. TOTAL NO. OF PAGES	7b. NO. OF REFS
29 February 1968	65	7

8a. CONTRACT OR GRANT NO.	9a. ORIGINATOR'S REPORT NUMBER(S)
N00014-67-C-0468	9204
b. PROJECT NO.	
c. TASK	9b. OTHER REPORT NO(S) *(Any other numbers that may be assigned this report)*
d. ARPA Order 306	

10. AVAILABILITY/LIMITATION NOTICES

"Qualified requestors may obtain copies of this report from DDC"

11. SUPPLEMENTARY NOTES	12. SPONSORING MILITARY ACTIVITY
	Advanced Research Projects Agency, The Office of Naval Research, Department of Defense

13. ABSTRACT

Internal filamentary glass damage caused by high power Q-switched pulse lasers and filamentary trapping in liquids is analyzed theoretically in this report. Several models are proposed and discussed for electrostrictively driven acoustic trapping. An analysis of Kerr effect trapping is also given for purposes of comparison.

In the acoustic theory, electrostriction is the sound wave driving force. The sound wave compressions cause focusing of the light wave fields. The focused light fields in turn cause stronger electrostriction forces. When the beam power is large enough and the laser pulse duration is approximately equal to the time required for sound to cross the unfocused beam radius, the trapping process runs until the beam is focused to a small radius limited by diffraction.

The theoretical trapping thresholds are calculated from the laser wavelength and the density, refractive index, Young's modulus, and Poisson's

(Continued)

DD FORM 1 JAN 64 1473

14. KEY WORDS	LINK A		LINK B		LINK C	
	ROLE	WT	ROLE	WT	ROLE	WT
Acoustic Trapping Electrostriction Kerr Effect Trapping Glass Damage Beam Trapping Sound-Light Interaction						

INSTRUCTIONS

1. ORIGINATING ACTIVITY: Enter the name and address of the contractor, subcontractor, grantee, Department of Defense activity or other organization *(corporate author)* issuing the report.

2a. REPORT SECURITY CLASSIFICATION: Enter the overall security classification of the report. Indicate whether "Restricted Data" is included. Marking is to be in accordance with appropriate security regulations.

2b. GROUP: Automatic downgrading is specified in DoD Directive 5200.10 and Armed Forces Industrial Manual. Enter the group number. Also, when applicable, show that optional markings have been used for Group 3 and Group 4 as authorized.

3. REPORT TITLE: Enter the complete report title in all capital letters. Titles in all cases should be unclassified. If a meaningful title cannot be selected without classification, show title classification in all capitals in parentheses immediately following the title.

4. DESCRIPTIVE NOTES: If appropriate, enter the type of report, e.g., interim, progress, summary, annual, or final. Give the inclusive dates when a specific reporting period is covered.

5. AUTHOR(S): Enter the name(s) of author(s) as shown on or in the report. Enter last name, first name, middle initial. If military, show rank and branch of service. The name of the principal author is an absolute minimum requirement.

6. REPORT DATE: Enter the date of the report as day, month, year, or month, year. If more than one date appears on the report, use date of publication.

7a. TOTAL NUMBER OF PAGES: The total page count should follow normal pagination procedures, i.e., enter the number of pages containing information.

7b. NUMBER OF REFERENCES: Enter the total number of references cited in the report.

8a. CONTRACT OR GRANT NUMBER: If appropriate, enter the applicable number of the contract or grant under which the report was written.

8b, 8c, & 8d. PROJECT NUMBER: Enter the appropriate military department identification, such as project number, subproject number, system numbers, task number, etc.

9a. ORIGINATOR'S REPORT NUMBER(S): Enter the official report number by which the document will be identified and controlled by the originating activity. This number must be unique to this report.

9b. OTHER REPORT NUMBER(S): If the report has been assigned any other report numbers *(either by the originator or by the sponsor)*, also enter this number(s).

10. AVAILABILITY/LIMITATION NOTICES: Enter any limitations on further dissemination of the report, other than those imposed by security classification, using standard statements such as:

(1) "Qualified requesters may obtain copies of this report from DDC."

(2) "Foreign announcement and dissemination of this report by DDC is not authorized."

(3) "U. S. Government agencies may obtain copies of this report directly from DDC. Other qualified DDC users shall request through

_____."

(4) "U. S. military agencies may obtain copies of this report directly from DDC. Other qualified users shall request through

_____."

(5) "All distribution of this report is controlled. Qualified DDC users shall request through

_____."

If the report has been furnished to the Office of Technical Services, Department of Commerce, for sale to the public, indicate this fact and enter the price, if known.

11. SUPPLEMENTARY NOTES: Use for additional explanatory notes.

12. SPONSORING MILITARY ACTIVITY: Enter the name of the departmental project office or laboratory sponsoring *(paying for)* the research and development. Include address.

13. ABSTRACT: Enter an abstract giving a brief and factual summary of the document indicative of the report, even though it may also appear elsewhere in the body of the technical report. If additional space is required, a continuation sheet shall be attached.

It is highly desirable that the abstract of classified reports be unclassified. Each paragraph of the abstract shall end with an indication of the military security classification of the information in the paragraph, represented as *(TS)*, *(S)*, *(C)*, or *(U)*.

There is no limitation on the length of the abstract. However, the suggested length is from 150 to 225 words.

14. KEY WORDS: Key words are technically meaningful terms or short phrases that characterize a report and may be used as index entries for cataloging the report. Key words must be selected so that no security classification is required. Identifiers, such as equipment model designation, trade name, military project code name, geographic location, may be used as key words but will be followed by an indication of technical context. The assignment of links, rules, and weights is optional.

13. ABSTRACT (Continued)

ratio of a solid material, or the density, refractive index, and speed of sound of a liquid medium. These thresholds agree with experimental glass damage thresholds to within experimental error, and they vary the same way with initial beam size. Computer movies showing the formation of strongly focused regions are presented. An explanation is given for most of the salient features observed in the damage phenomenon. Mathematical analyses of various features of the models are presented with computed graphs.